2016

Investigation of the Critical Role of Polymeric Binders for Silicon Negative Electrodes in Lithium-Ion Batteries

Jiagang Xu
University of Kentucky, jg.xu@uky.edu
Author ORCID Identifier:
http://orcid.org/0000-0002-2736-1733
Digital Object Identifier: https://doi.org/10.13023/ETD.2016.437

STUDENT AGREEMENT:

I represent that my thesis or dissertation and abstract are my original work. Proper attribution has been given to all outside sources. I understand that I am solely responsible for obtaining any needed copyright permissions. I have obtained needed written permission statement(s) from the owner(s) of each third-party copyrighted matter to be included in my work, allowing electronic distribution (if such use is not permitted by the fair use doctrine) which will be submitted to UKnowledge as Additional File.

I hereby grant to The University of Kentucky and its agents the irrevocable, non-exclusive, and royalty-free license to archive and make accessible my work in whole or in part in all forms of media, now or hereafter known. I agree that the document mentioned above may be made available immediately for worldwide access unless an embargo applies.

I retain all other ownership rights to the copyright of my work. I also retain the right to use in future works (such as articles or books) all or part of my work. I understand that I am free to register the copyright to my work.

REVIEW, APPROVAL AND ACCEPTANCE

The document mentioned above has been reviewed and accepted by the student's advisor, on behalf of the advisory committee, and by the Director of Graduate Studies (DGS), on behalf of the program; we verify that this is the final, approved version of the student's thesis including all changes required by the advisory committee. The undersigned agree to abide by the statements above.

Jiagang Xu, Student

Dr. Yang-Tse Cheng, Major Professor

Dr. Thomas Dziubla, Director of Graduate Studies

INVESTIGATION OF THE CRITICAL ROLE OF POLYMERIC BINDERS FOR SILICON NEGATIVE ELECTRODES IN LITHIUM-ION BATTERIES

DISSERTATION

A dissertation submitted in partial
fulfillment of the requirements for
the degree of Doctor of Philosophy
in the College of Engineering at the
University of Kentucky

By
Jiagang Xu
Lexington, Kentucky

Director: Dr. Yang-Tse Cheng, Professor of Chemical and Materials
Engineering
Lexington, Kentucky 2016

ABSTRACT OF DISSERTATION

INVESTIGATION OF THE CRITICAL ROLE OF POLYMERIC BINDERS FOR SILICON NEGATIVE ELECTRODES IN LITHIUM-ION BATTERIES

Silicon is capable of delivering a high theoretical specific capacity of 3579 mAh g^{-1}, which is about 10 times higher than that of the state-of-the-art graphite-based negative electrodes for lithium-ion batteries (LIBs). However, the poor cycle life of silicon electrodes, caused by the large volumetric strain during cycling, limits the commercialization of silicon electrodes. As one of the essential components, the polymeric binder is critical to the performance and durability of lithium-ion batteries as it keeps the integrity of electrodes, maintains conductive path and must be stable in the electrolyte. The guideline for binder selection of silicon electrodes is still not available as the electrochemical performance of silicon is very challenging and lots of research are still being carried out.

This dissertation is focused on unveiling the critical role of polymeric binders in silicon negative electrodes. As a first step, silicon electrodes mixed with commercially available Nafion and ion-exchanged Nafion were demonstrated to maintain a high specific capacity over 2000 mAh g^{-1} cycled between 1.0 V and 0.01 V, compared with the traditional binder polyvinylidene fluoride (PVDF). Stable cycling at 1C rate for more than 500 cycles was achieved by limiting the lithiation capacity to 1200 mAh g^{-1}.

Secondly, a comprehensive study of the binding mechanisms of these binders in silicon/$LiNi_{1/3}Mn_{1/3}Co_{1/3}O_2$ full cells was carried out by using techniques such as X-ray photoelectron spectroscopy (XPS) and instrumented nanoindentation. Partial charge/discharge testing with controlled silicon lithiation capacity showed that the ion-exchanged Nafion and sodium alginate were both effective binders to maintain 1200 mAh g^{-1} for a long period of cycling without capacity decrease. Full charge/discharge testing showed that the ion-exchanged Nafion and sodium alginate binders exhibited the highest capacity retention when the volume change of silicon nanoparticles was about 300%.The superior performance of ion-exchanged Nafion was due to its capability to conduct Li^+ to isolated silicon nanoparticles. Binders would not affect the composition of solid electrolyte interphase (SEI). Therefore, coupled chemical degradation (SEI growth, lithium consumption) and mechanical degradation (cracking, particles isolation) are the cause of the failure of the full cells.

KEYWORDS: Silicon, polymer binder, Nafion, lithium-ion batteries, full cell

Author's signature: Jiagang Xu

Date: November 25, 2016

INVESTIGATION OF THE CRITICAL ROLE OF POLYMERIC BINDERS FOR SILICON NEGATIVE ELECTRODES IN LITHIUM-ION BATTERIES

By
Jiagang Xu

Director of Dissertation: Dr. Yang-Tse Cheng

Director of Graduate Studies: Dr. Thomas Dziubla

Date: November 25, 2016

Dedicated to my family

ACKNOWLEDGMENTS

My graduate studies and life in UK have benefited from many great people. I appreciate everyone sincerely, and may not list all of them here:

First of all, I would like to express great gratitude to my advisor Prof. Yang-Tse Cheng. Without his instructions, understanding and encouragement in the past several years, I may not go this far. Secondly, I want to extend my gratitude to the research group members (*former* and current) for their invaluable assistance, such as *Juchuan Li*, *Rutooj Deshpande*, *Qinglin Zhang*, *Jie Pan*, Mohanad Al-Shroofy, Tao Chen, Long Zhang, Yikai Wang, and Jiazhi Hu. Other colleagues and staff I may request experimental assistance from are Nicolas Briot and Dali Qian from the Electron Microscopy Center and Yiyang Liu from Department of Chemistry.

Specially, I want to thank Dr. Vincent Battaglia for the support of a short summer visit to the Berkeley lab in 2013, which was very useful for my research afterwards.

Thanks to staff in the department for their patience, understanding and assistance. Thanks to Prof. Rodney Andrews from Center for Applied Energy Research, Prof. John Balk and Prof. Matthew Beck from the Materials Engineering Program, and Prof. John Selegue from Department of Chemistry for serving as my dissertation committee members. I appreciate their advices as well.

Most importantly, thanks to the birth of my nephew who brings lots of happiness to my family and thanks to my brother taking care of our parents when I am away from home.

Finally, I would like to thank the financial support from National Science Foundation (Award numbers: 1000726, 1355438).

TABLE OF CONTENTS

LIST OF FIGURES

LIST OF TABLES

Chapter 1 Introduction

Fossil fuels are not inexhaustible and pollutants released by burning fossil fuels are damaging the environment nowadays. Therefore, renewable energy sources, such as hydro, wind, solar and nuclear energy, are important for sustainable development. Energy can be stored and used afterwards in many ways, for example, hydroelectric energy can be treated as mechanical energy storage because the potential energy of water is stored before electricity can be generated. Similarly, electrochemical energy storage refers to systems that can convert chemical energy stored in chemical species to electrical energy through electrochemical reactions. These systems are generally called batteries.

There are many types of batteries, including nonrechargeable and rechargeable batteries, among which we can see alkaline, lead-acid, nickel-metal hydride (Ni-MH) and lithium-ion batteries (LIBs) quite often in our everyday life. Batteries usually consist of one or more cells, and each cell is mainly composed of the negative electrode, the positive electrode and the electrolyte.

Since LIBs were commercialized in 1991, they were widely used in small, portable electronic devices due to high energy density, high power discharge capability, high voltage, low self-discharge rate and long cycle life. Currently, graphite and lithium metal oxides are used as the negative electrode and positive electrode for commercial mass production of LIBs. Additionally, pure electric vehicles powered by LIBs have been successfully commercialized by various automobile companies including Tesla and Nissan in the past few years. However, there are incentives to development new electrode materials to further lower the cost of batteries. For example, there are many choices for the negative electrode as many metallic elements can store more lithium than the carbonaceous negative electrode. But the poor cycling ability is a common

problem of those high capacity electrodes.

Silicon is able to deliver a theoretical capacity of 3579 mAh g^{-1} based on the alloy $Li_{15}Si_4$ formed at room temperature, which is about ten times of that of the graphite electrode. So far, substantial research and development investment had been made to the advancement of the commercialization of silicon-based negative electrodes.

This dissertation is focused on study of the critical role of polymeric binders to better understand the failure mechanism of nanoparticle silicon electrodes and to provide insights to overcome the poor cycling performance of silicon electrodes. As the first chapter, to lay a solid foundation for my work, a comprehensive summary of those important aspects of advancing LIBs is presented below:

1.1 Fundamentals of Lithium-Ion Batteries

The working mechanism of LIBs is lithium inserts into and moves out of either the negative electrode or positive electrode reversibly. In general, a single Li-ion cell can generate a voltage more than 3.5 V. As shown in Figure 1.1, a typical Li-ion cell is composed of the negative electrode, positive electrode, separator, and organic electrolyte. The well-known graphite has a layered structure, which allows lithium to stay between carbon layers. While for the positive electrodes, $LiCoO_2$, $LiMn_2O_4$, and $LiFePO_4$ have the layered, spinel, and olivine structure respectively. The derivatives of these oxides generally share the similar crystalline structures. The separator (porous membrane, e.g., polypropylene) is used to prevent the direct contact between two electrodes. The electrolyte contains lithium salts dissolved in organic solvents and it is playing the roles of electronic insulator and ionic conductor. Although the electrolyte can be liquid, solid, or polymer gel, nonaqueous electrolyte typically refers to lithium salts (e.g., $LiPF_6$) dissolved in a mixture of organic solvents (e.g., ethylene carbonate and diethyl carbonate) and other additives.

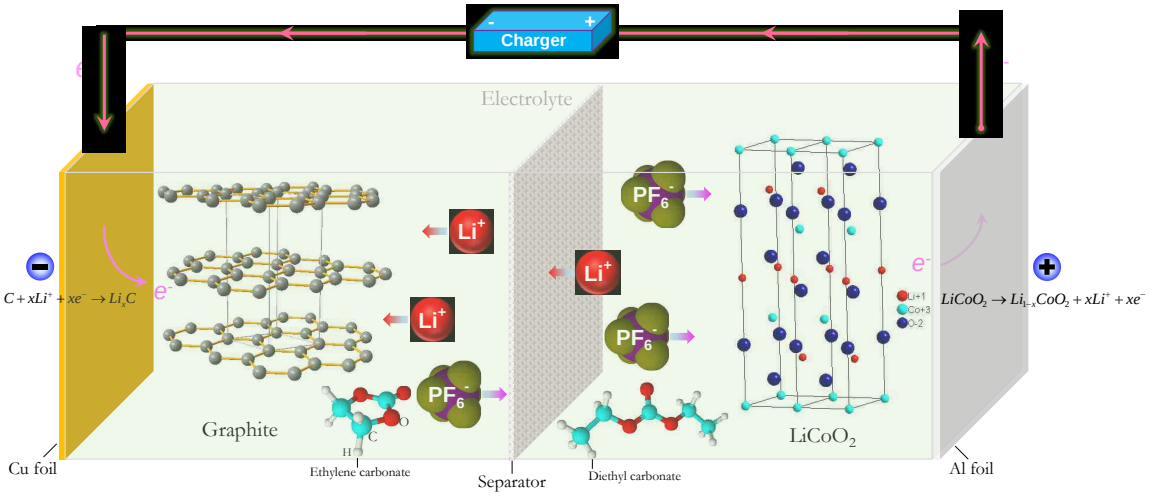

Figure 1.1: Structure of a Li-ion cell during charging.*

In Figure 1.2, a half cell consists of the working electrode (research object) and counter/reference electrode (lithium metal). A full cell consists of the negative electrode and positive electrode, which are both research objects. In this dissertation, discharge means the cell is connected to a load and lithium leaves the counter/reference electrode or negative electrode (i.e. oxidation) to react with the working electrode or positive electrode (i.e. reduction). This process is also commonly called lithiation/intercalation in the half cells. Charge means the cell is connected to an external power source and the reverse process will happen. Charge process is also called delithiation in the half cells.

For a spontaneous chemical reaction, the standard reaction Gibbs free energy should be less than zero. Similarly, in an electrochemical cell, the driving force of an overall electrode reaction is the decrease of the Gibbs free energy of the system. Assume the negative electrode is graphite and positive electrode is $LiMO_2$ (M can be

*All the schematics in this dissertation are drawn in PowerPoint 2013. In Figure 1.1, structures of the electrodes and electrolyte components are obtained from the free versions of Diamond 4.0 and ChemSketch 12.0 respectively.

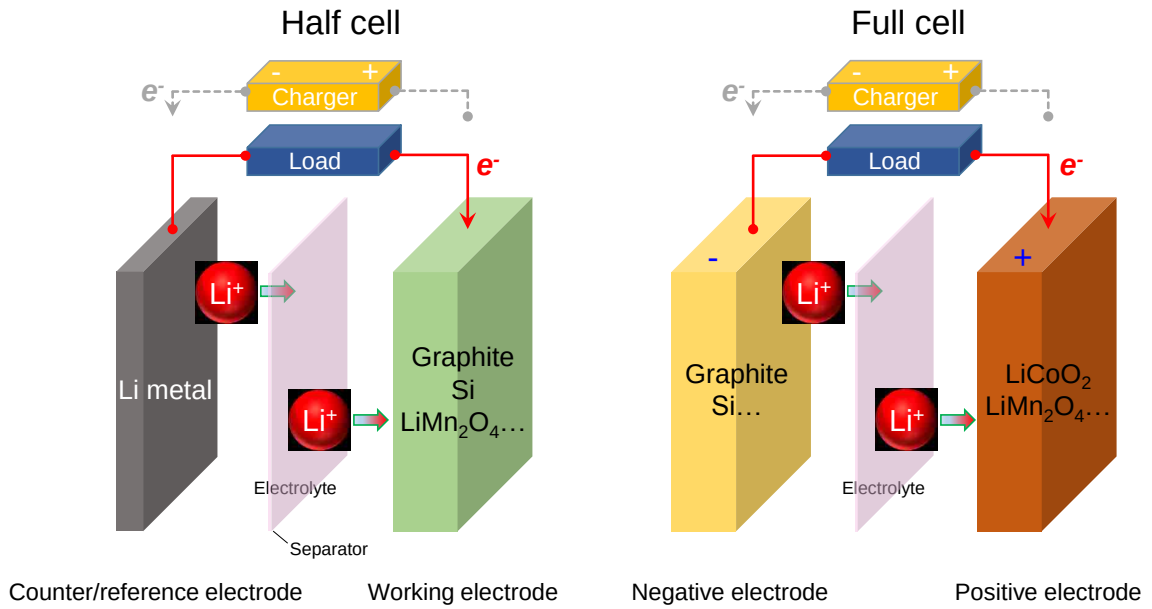

Figure 1.2: Terminology related to Li-ion cells. The schematic shows the discharge process. Gray dash lines connected with chargers indicate the charge process.

Co, Ni, Mn, etc.), electrode reactions are [1]

$$\text{Negative electrode: } C + xLi^+ + xe^- \longleftrightarrow Li_xC \tag{1.1}$$

$$\text{Positive electrode: } LiMO_2 \longleftrightarrow Li_{1-x}MO_2 + xLi^+ + xe^- \tag{1.2}$$

$$\text{Overall: } C + LiMO_2 \longleftrightarrow Li_{1-x}MO_2 + Li_xC \tag{1.3}$$

And the theoretical standard open circuit potential E (in volt) is determined by [2]

$$\Delta G = -nFE \tag{1.4}$$

Where n is the number of electrons involved in the electrode reaction, G is the standard free energy (driving force) in J mol^{-1}, F is the Faraday's constant (96485 C mol^{-1}, or 26801.5 mAh mol^{-1}).

Based on the experimental results, for graphite and silicon, the midpoint voltages

versus lithium are round 0.1 V, while for the lithium metal oxides, the midpoint voltages versus lithium are generally more than 3.4 V [1]. Therefore, the high voltage of LIBs indeed comes from the positive electrode.

The specific capacity of either the negative electrode or positive electrode can be calculated as the total charge per unit mass of electrode materials based on the corresponding electrode reaction when the most saturated phase is formed with lithium. The formula for calculating the specific capacity (in mAh g^{-1}) of a single active material is

$$\text{Specific capacity} = \frac{nF}{M} \tag{1.5}$$

Where n is the number of electrons involved in a single electrode reaction, F is the Faraday's constant, M is the molar mass of active material in g mol^{-1}.

It is not difficult to calculate the theoretical capacities for some common electrode materials based on above equation, for example, 372 mAh g^{-1} for LiC_6, 3579 mAh g^{-1} for $Li_{15}Si_4$, 278 mAh g^{-1} for $LiNi_{1/3}Mn_{1/3}Co_{1/3}O_2$ (NMC). The specific capacities and volumetric capacities (mAh L^{-1}) for some elements are calculated in Table 1.1. So we can learn that silicon has the highest specific capacity and volumetric capacity. Other important ratings of LIBs, such as the specific energy (Wh kg^{-1}) and energy density (Wh L^{-1}), can be obtained in a similar way when voltages are specified. In fact, for real batteries, the weight and volume of other components of batteries are also taken into the calculations of various ratings.

Table 1.1: Specific capacities and volumetric capacities for some elements.

Material	Phase	Specific capacity mAh g^{-1}	Volumetric capacity mAh mL^{-1}	Density g cm^{-3} [3]	Molar mass g mol^{-1} [3]
C	LiC_6	372	781	2.27	12.01
Zn	LiZn [4]	410	2927	7.14	65.39
Ga	Li_2Ga	769	4545	5.91	69.72
Sn	$Li_{22}Sn_5$ [4]	993	7249	7.30 (white)	118.71
Al	LiAl [5]	993	2681	2.70	26.98
Si	$Li_{15}Si_4$	3579	8339	2.33	28.08

The specific capacity of pure lithium can be obtained as 3862 mAh g^{-1} when $n = 1$ and the molar mass $M = 6.94$ g mol^{-1}. Even though the lithium has a very high capacity, however, it has never been used as the negative electrode commercially due to the safety concern, which is the lithium dendrites formed during operation may short-circuit the cell.

1.2 Development of Negative Electrode Materials

1.2.1 Carbonaceous Negative Electrode

Carbonaceous materials, such as graphite and petroleum coke (one type of soft carbons), were used in batteries long time ago [6]. Specially, graphite has a layered structure held together by van der Waals forces and lithium will stay between carbon layers upon charge/discharge. Maximum concentration of lithium in graphite is one lithium per six carbon atoms (LiC_6), and the theoretical capacity is 372 mAh g^{-1} as mentioned earlier. The volume change when lithium inserts into graphite is less than 10% [7][8], which makes graphite successfully used for commercial batteries requiring stable operation and long cycle life. Furthermore, lithiation capacity, mechanism and electrochemical performance are strongly dependent on the structure and composition of carbonaceous materials [7]. The capacity as high as 437 mAh g^{-1} of the doped carbon film electrode was obtained by substituting the carbon with boron [9].

Another type of soft carbon named mesocarbon microbeads (MCMB) was shown promising electrochemical behavior as well [10][11]. MCMB are of spherical shape and have low specific surface area, which could reduce the amount of side reactions during cycling. As an allotrope of carbon, single-walled carbon nanotubes have been proved to increase the initial capacity up to 1000 mAh g^{-1} [12]. Carbon nanotubes can offer higher conductivity and higher tensile strength compared with graphite. They can also be used as the support matrix to form composites with other high capacity materials, which can reduce cracking of active materials as carbon nanotubes are

playing the roles of gluing other coated particles together and transporting electrons [13]. The practical performance of carbon nanotubes varies with their structures, defects and electronic properties. The relatively large irreversible capacity loss after the 1^{st} cycle and lack of voltage plateau during discharge are believed to limit the real applications of carbon nanotubes.

1.2.2 Alloy Negative Electrode

Besides Li-C system, there are many other metallic lithium alloys with higher specific capacities studied for the alternative negative electrode materials, such as, Li-Sn [4][5][14][15], Li-Ge [16][17], and Li-Ga [18]-[21]. As shown in Table 1.1, LiAl and $Li_{22}Sn_5$ have the same specific capacity of 993 mAh g^{-1}. But they have very different volumetric capacities. Different from graphitic materials, lithium is not stored between carbon layers anymore, but forms alloys with metallic elements. Intermetallics were also used as the negative electrode materials due to their relatively high capacities, such as Sn/SnSb [15][22]. As each metal atom can alloy with more than one lithium atom, metallic electrodes have higher capacities. However, significant volumetric expansion occurs during cycling, which leads to the pulverization of active material particles, electric contact loss and permanent capacity loss upon cycling. Another reason of capacity decay of the intermetallic electrodes is that the solid electrolyte interphase (SEI) layer formed at the electrode-electrolyte interface will also experience large mechanical strain and continued growth of this SEI layer would contribute to the irreversible capacity loss as well [22]. Beaulieu *et al.* observed the huge volume changes of amorphous alloy electrodes, and concluded that the intermetallic electrodes had no potential application in batteries due to the poor capacity retention caused by cracking [23]. Other than pure metallic elements and alloys, metal oxides, such as $Li_4Ti_5O_{12}$ with a spinel structure, can also react with lithium to be used as the negative electrode, which prevents lithium dendrites formation as well

as maintains very good cycle life [24]-[28]. The disadvantage of $Li_4Ti_5O_{12}$ is its high voltage of about 1.5 V versus lithium, which can lower the energy density compared with graphite.

1.2.3 Silicon Negative Electrode

Compared with other elements, silicon is the most promising candidate for negative electrode material to satisfy future needs, as it has the highest theoretical capacity, 4200 mAh g^{-1} (based on the most saturated phase $Li_{22}Si_5$) [5][29][30], which is more than ten times of that of graphite. Based on $Li_{15}Si_4$, the capacity is 3579 mAh g^{-1}. Nowadays, research about silicon negative electrodes towards better performance is one of those hottest topics in the field of energy storage and getting more attention even if the insertion behavior of Li-Si alloy has been studied in the last century [31]. Similar to many other single elemental or alloy electrodes mentioned before, during lithiation, silicon electrodes also have bad performance due to the large volume change (as high as 310%) [32]. Large volume expansion and associated stress lead to pulverization of electrodes and capacity loss. There are many approaches to overcome the large volume change and to obtain better capacity retention and they can be summarized as: nano-sized silicon powers; silicon dispersed in inactive/active matrix; silicon electrode with different binders; silicon thin films [30][33]. In general, the specific capacity of silicon thin film electrode is limited as the thickness is within several hundred nanometers range. Studies of silicon thin film [34][35] and nanostructured silicon [36]-[38] have shown improvements of the cycle life. For instance, double-walled silicon nanotube has very stable cyclic behavior, good rate capability and very higher capacity (more than 600 mAh g^{-1}) than those of carbon-based negative electrodes by controlling the SEI layer formation at the silicon-electrolyte interface [39]. The mechanical layer coated around silicon nanotube was made of SiO_x and it could prevent the nanotube from expanding during lithiation and therefore

guaranteed the stability of the SEI layer.

1.2.4 Composite Negative Electrode

By utilizing the features of individual components, composite electrodes are introduced as the promising negative electrodes in LIBs. Graphite has very good cycling stability and tin has high capacity. High energy ball-milled graphite-tin composite electrode was reported to deliver capacity around 800-1250 mAh g^{-1} at the first cycle with large amount of capacity decay afterwards [40]. Another mechanical ball-milled composite composed of silicon (21.6 wt%), graphite (64.8 wt%), and polyacrylonitrile-based disordered carbon (13.6 wt%) was shown to exhibit a capacity of about 660 mAh g^{-1} and good capacity retention for more than 30 cycles [41]. High reversible capacity ($\sim$ 1000 mAh g^{-1}) and long cycle life were achieved by using nano-sized silicon (pyrolysis process of monosilane)/graphite composite electrode [42]. Additionally, when carbon nanofibers were coated with amorphous silicon by the chemical vapor deposition method, the carbon core provides electron pathways and mechanical support while having limited volume expansion. This kind of core shell structure can deliver capacity up to 2000 mAh g^{-1} [43].

1.3 Development of Positive Electrode Materials

For LIBs, positive electrode materials are typically lithiated metal oxides. They are required to have high free energy when reacting with lithium, to maintain crystal structures after lithiation/delithiation and to be compatible with other components in the cell [1]. Overall, factors like specific capacity, rate capability, high temperature behavior, safety, cost and processing determine the real application of positive electrodes.

Positive electrodes in the market have three basic structures: layered structure (e.g., $LiCoO_2$), spinel structure (e.g., $LiMn_2O_4$) and olivine structure (e.g., $LiFePO_4$).

$LiCoO_2$ is the most commonly used positive electrode material in small-scale consumer electronics because of its high operating voltage ($\sim$ 4 V), easy processing and good cycle life [44]. Theoretical capacity of $LiCoO_2$ is 274 mAh g^{-1}, while the practical capacity is only about 140 mAh g^{-1} due to the structural and chemical instability (Co dissolved in electrolyte) at deep discharge when $x > 0.5$ ($Li_{1-x}CoO_2$) [45][46]. Since Co is toxic and less abundant than other metals (such as Mn and Fe), $LiMn_2O_4$ and $LiFePO_4$ were developed to enhance the safety and reduce the cost. Solid solutions $LiNi_xMn_yCo_zO_2$ were also extensively studied for their high capacity, good rate capability and high voltages [47]-[51]. Based on previous basic structures, doping elements (e.g., Al, Ni, Ti, Mg, Zr) were commonly introduced to the mentioned positive electrode materials to either reduce capacity loss or improve capacity retention [52]. Overall, performances of positive electrode materials are related to electrode microstructure, particle size or shape and surface modification. More characteristics and research progress of various positive electrode materials can be found in references [1][44][52]-[54].

So far, as we know, practical specific capacity of the positive electrode is much lower than that of the negative electrode. The overall capacity of a cell is in fact limited by the positive electrode. Therefore, we are still facing challenges of lowering the cost and increasing the energy and power densities, especially, for positive electrode materials.

1.4 Development of Polymeric Binders

Current commercial LIBs electrodes are composed of graphite/$LiCoO_2$, binder (polyvinylidene fluoride, PVDF) and conductive carbon. In fact, polymers (e.g., poly(ethylene oxide), PEO) were widely studied in lithium polymer batteries long time ago [55]-[57]. For LIBs, the importance of binder began to show up as people were studying novel alloy and silicon electrodes. Chen *et al.* reported crosslinked elastomeric

polymer could be used to maintain good capacity retention for amorphous Si-Sn electrodes in spite of the 125% volume change [58]. Sodium carboxymethyl cellulose and lithium ion exchanged Nafion were reported to have improved performance for crystalline silicon powders (size, 44 μm) [59][60]. Conductive binder without adding conductive carbon black in the electrode was proved to accommodate silicon volume change, and high capacity and long term cycling were also achieved [61]. We are aware of the basic role of binder is to hold electrode particles together and adhere the whole electrode well to the current collector, because once electrode particles are not involved in electron transfers, the capacity decay will start. There may be interactions among binder, electrolyte, carbon black and active materials. The ability of electrolyte uptake and uniform distribution of carbon black could contribute to the performance of batteries. For electrodes experiencing large volume changes, an ideal binder is supposed to tolerate the volume change, maintain good ionic conductivity and be chemically stable in the operating voltage window [62].

1.5 Failure Mechanisms of Electrodes

Understanding the mechanism of aging of LIBs is extremely important, as it has strong relations with the manufacturing of batteries, development of new components (negative electrode, positive electrode, electrolyte, etc.) of batteries, storage of batteries, environmental control of battery operations and final applications. We know LIBs have been widely used in portable devices. These devices have relatively short life and aging of batteries after certain period of usage doesn't show too much importance. However, for future market of electric vehicles applications, 10-15 years lifetime and up to 1000 cycle life with at least 80% capacity retention are required [63].

Even if the research about developing new electrodes are going around worldwide, carbon based graphite is still the best candidate for the negative electrode so far.

Generally, the aging effects of carbon based negative electrodes can be summarized as: SEI layer formation at the beginning of cycling and continued growth of the SEI layer during storage and cycling [64]. For positive electrodes made of lithium metal oxides, aging of active materials themselves, oxidation of electrolyte components, interactions with negative electrodes and structural changes during cycling were believed to affect the lifetime and capacity [64]. Since battery systems are very complex to understand, the aging mechanism usually depends on the specific system. For example, the fading mechanisms of positive electrodes made of $LiMn_2O_4$ (spinel structure) include structural change due to Jahn-Teller distortion of Mn^{3+} [65][66] and dissolution of Mn^{2+} in the electrolyte at low state of charge and electrolyte oxidation and instability of delithiated lithium manganese spinel at high state of charge [64].

To predict the cycle life and study the capacity fading mechanism quantitatively over a long period, numeric modeling and experiments were investigated by many groups [67]-[70]. Generally, chemical degradation was defined as the side reactions and formation of the SEI due to the decomposition of electrolyte on electrode surfaces. This is the main cause of lithium loss. Most cycle life models consider chemical degradation as the major capacity fading mechanism [71][72]. On the other hand, mechanical degradation driven by stress and strain fields during lithiation and delithiation also contributes to the capacity fading. At the same time, cracking of active material particles resulted from the large stress will facilitate the side reactions. There are many efforts in literatures to predict the stress generation upon cycling in a single electrode particle by assuming simple geometries [73]-[79]. Real time stress measurement was carried out on the graphite electrode bonded with silicon wafer substrate by monitoring the curvature change of wafer during electrochemical cycling [80].

1.6 Design of Real Batteries

Half cells are commonly used in laboratories, in which either the negative electrode or positive electrode is assembled against pure lithium reference electrode. Practical batteries (full cells) are consisted of negative electrode and positive electrode though. Unlike infinite supply of lithium atoms in half cells, lithium is stored in positive electrode only in full cells. One of the advantages of using half cells is we can study the electrochemical behaviors of either the negative electrode or positive electrode separately.

There are many parameters could affect the performance of real batteries, such as the electrode thickness, electrode porosity/density, inactive additives [81]-[86]. Appropriate electrode thickness is critical to the electrochemical performance and cycleability. There is a gap between the theoretical capacity and practical capacity of electrodes in LIBs system due to the limited electronic and ionic conductivities of active materials [87]. Although this gap could be narrowed by adding other conductive additives, these additives may affect specific properties by occupying mass and space inside electrodes and impair the liquid transport speed and high rate performance. Study of the cooperation between the positive electrode $LiN_{0.8}Co_{0.15}Al_{0.05}O_2$, PVDF and conductive acetylene black (AB) shows an optimal ratio of PVDF to AB (5:3, by weight) can be obtained considering the ion blocking effect of PVDF and electronic conducting effect of AB [88]. And also, if the amount of PVDF and AB is too small, long cycle tests show the mechanical integrity of electrode may become a problem. On the other hand, the ratio of PVDF to AB plays an important role of optimizing the interfacial resistance and higher PVDF content is believed to reduce the charge transfer resistance by improving the local electronic conductivity [89].

Another important factor for full cells is the capacity balancing of electrodes. Reports mentioned electrodes balancing or the negative electrode/positive electrode mass ratio have come out shortly after LIBs were commercialized [90]-[92]. Over-

charge of the graphite would happen if the negative electrode capacity is less than that of the positive electrode capacity, which causes lithium deposition (dendrite) on the negative electrode surface [93][94]. Excess negative electrode materials will increase materials cost and cause low capacity and Coulombic efficiency due to the side reactions such as the formation of SEI layer. In general, to reach maximum capacity and avoid lithium deposition, the negative electrode should have a little more capacity to match the positive electrode after subtracting the capacity loss due to the SEI formation [86].

Chapter 2 Experimental Methods

Battery research in laboratories using two electrodes can be conducted in commercial coin cells, pouch cells, cylindrical cells, Swagelok-type cells and many other customized systems. Commercial coin cells are chosen in my work because of the high reproducibility and relatively low cost. A schematic plot of the structure of a CR2025 coin cell with a diameter of 20 mm and a thickness of 2.5 mm is shown in Figure 2.1. The plastic gasket is used to separate the cap and case. The porous separator made of polymers immersed in the electrolyte is used to conduct ions and to prevent short circuit. The spring made of stainless steel is necessary to secure the components inside when the cell is sealed. The spacer made of stainless steel is essential for protecting the electrode against the spring.

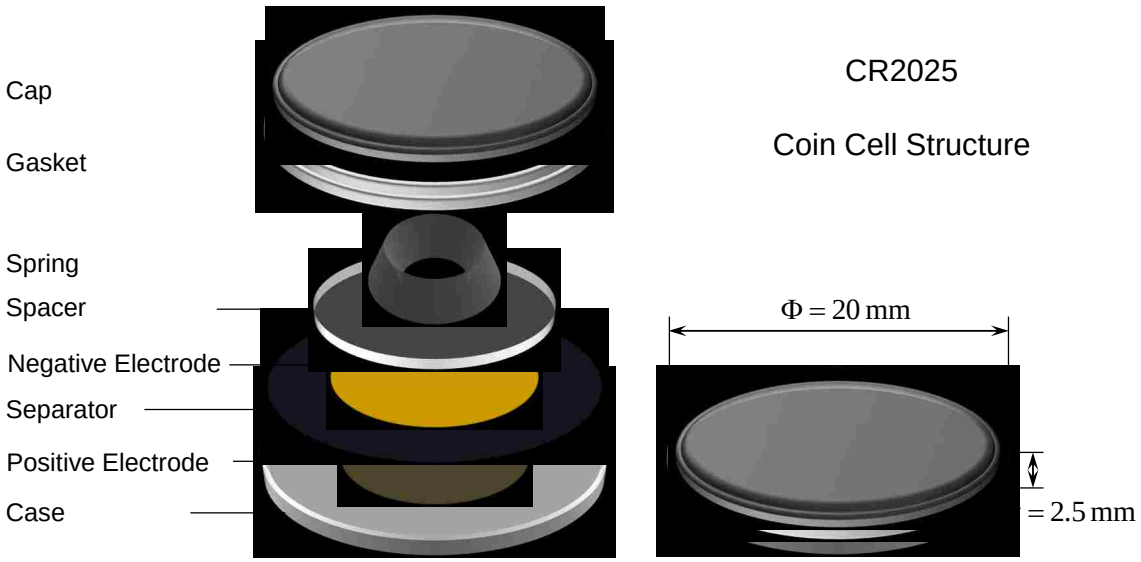

Figure 2.1: CR2025 coin cell structure.

As mentioned in Section 1.1, using either half cell or full cell is dependent on the research objectives. In a half cell, the working electrode is placed on the case

and a piece of lithium foil disk is placed above the separator. In a full cell, the positive electrode is placed on the case and the negative electrode is placed above the separator as shown in Figure 2.1. The diameter of the negative electrode or lithium disk is usually a bit larger than that of the positive electrode or working electrode to ensure a good alignment.

Typical porous LIB electrodes are made from powders of the electroactive materials, polymer binders and conductive additives. Powders are blended in a container using the solvents of binders to control the viscosity. Finally, the slurry is coated on a piece of thin current collector, such as copper or aluminum foil. After drying, the electrode may need to go through a rolling press to control the density and porosity. In some cases, electrodes are coated on both sides of the current collector to increase the energy density. Figure 2.2 shows a schematic plot of fabricating electrodes in the lab.

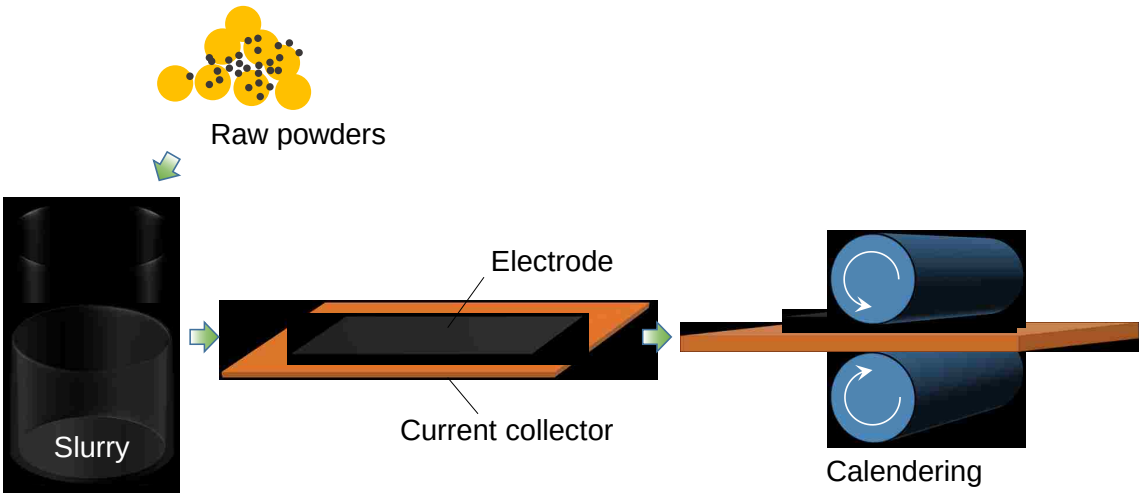

Figure 2.2: LIB electrodes fabrication procedure.

Some common parameters for the electrodes are discussed here: the loading of the electrode is expressed as the mass of active material per unit disk area in g cm^{-2} or the capacity per unit disk area in mAh cm^{-2}. High loading generally means high

energy density. The electrode density is defined as the ratio of the mass to the actual volume (product of the thickness and the area) of the electrode. When the density of each powder and mass of each electrode are known, the theoretical volume of the electrode can be obtained. Thus the porosity of the electrode ϕ can be calculated from this equation:

$$\phi = \frac{V_{actual} - V_{theoretical}}{V_{actual}} \tag{2.1}$$

The reliability of electrochemical measurement result is highly dependent on the quality of electrodes. High quality electrodes require delicate work at every step. For instance, electrodes must be dried thoroughly to remove moisture and the glove box for coin cell assembly must be kept in good condition all the time. Before test, the uniformity of a piece of electrode laminate can be assessed from the thickness and mass distribution of electrode disks.

Several essential characterization techniques used in my work are discussed briefly in the following sections, including my data only:

2.1 Structural Determination and Surface Morphology

For battery studies, X-ray diffraction (XRD) technique is commonly used to identify the crystalline structures of the synthesized negative and positives electrodes. Additionally, X-ray *in situ* experiments could give information of what crystalline phases are formed during cycling test [19]. Scanning electron microscope (SEM) is a powerful tool to study the microstructures. The surface morphology and changes after electrochemical evaluation are very useful for understanding the failure mechanisms of electrodes. With the help of energy dispersive X-ray (EDS) equipment attached to a SEM, it's also convenient to get the chemical compositions of synthesized materials or new materials formed on electrodes after electrochemical reactions.

2.2 Electrochemical Measurement

2.2.1 Constant Current Cycling and Constant Voltage Charge/Discharge

Galvanostatic cycling with potential limitation (GCPL), or simply called cycling, is widely used to obtain capacities, power characteristics and cycle life of batteries quantitatively by running a series of charge and discharge sequences under constant currents between potential limits. It is expected to see batteries can maintain their properties (e.g. 80% capacity retention) after a long period of usage. By varying the input currents, we can obtain the capacity data under the slow or fast charge/discharge rates (i.e. C-rates). C-rate is a constant current require to charge/discharge a cell in a specified period of time. For example, C/10 means the current under which charge/discharge takes 10 hours to complete. This is also named the rate performance of a battery. From voltage versus capacity (or time) curves, named voltage profiles as illustrated in Figure 2.3, lithiation/delithiation reactions happening on electrodes can be understood with the resources of phase diagrams and thermodynamics theories [95]. The voltage window for the practical usage of LIBs is also determined by the GCPL technique. Moreover, real batteries are pre-cycled to stabilize the capacity and Coulombic efficiency after assembling.

Figure 2.3(a) shows eight charge (2.0→4.2 V) and discharge (4.2→2.0 V) cycles of the $LiNi_{1/3}Mn_{1/3}Co_{1/3}O_2$ (NMC111) electrode after a half cell was assembled. It is apparent that the feasible voltage is more than 3.5 V. Figure 2.3(b) shows a complete discharge (1.0→0.005 V) and charge (0.005→1.0 V) cycle for the graphite electrode in a half cell. The three plateaus around 0.2 V, 0.11 V and 0.07 V are the feature of the graphite electrode, corresponding to the two-phase regions LiC_{72}+LiC_{36}, LiC_{36}+LiC_{18} plus LiC_{18}+LiC_{12}, and LiC_{12}+LiC_6 respectively [6]. If there is a graphite/NMC111 full cell with balanced capacities, the voltage profile will be the combination of two curves shown in Figure 2.3, as the overall voltage is equal to the voltage difference

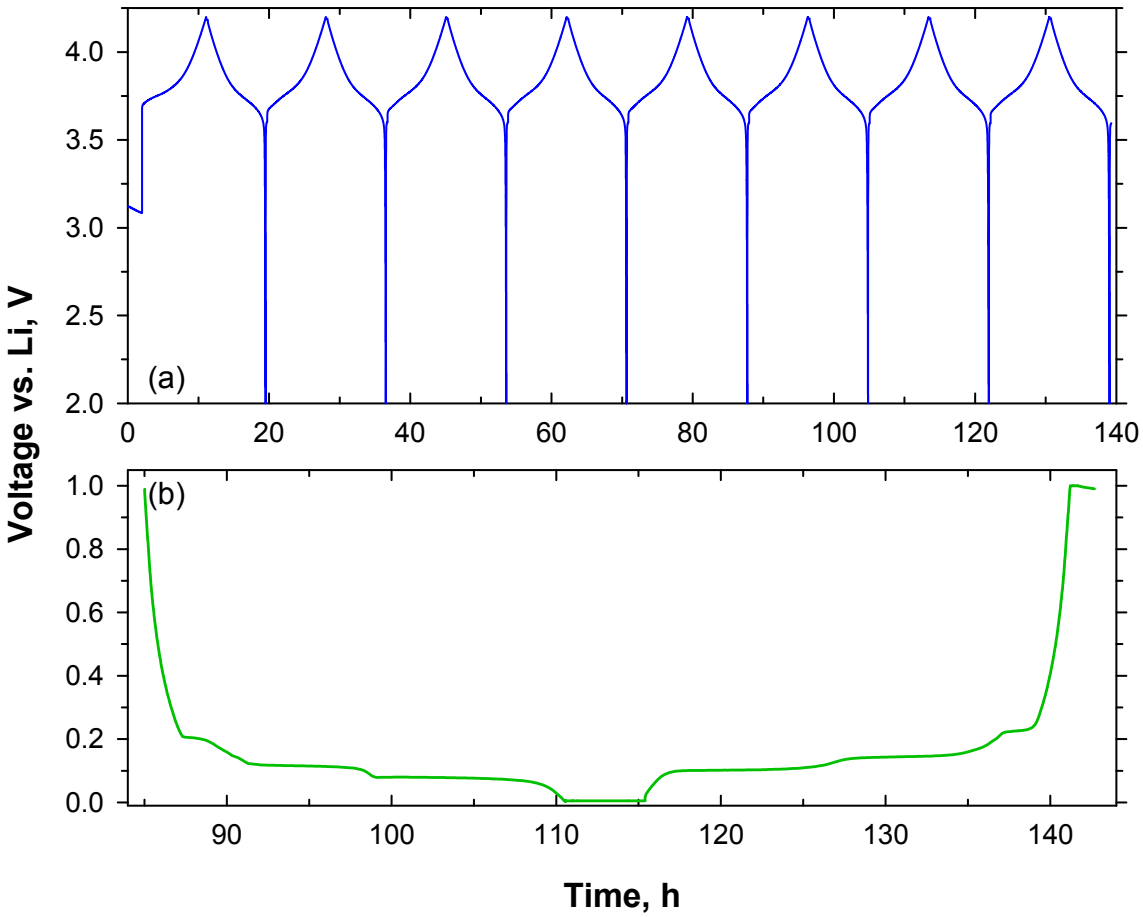

Figure 2.3: Constant current cycling of the NMC111 (a) and graphite (b) electrodes in lithium-ion half cells.

of the two electrodes. If necessary, the addition of the 3^{rd} electrode (also named reference electrode) will help discriminate the electrode reactions.

Constant voltage charge/discharge technique is generally used to maximize the electrode reactions during which the voltage is keeping constant and the current is decreasing. In Figure 2.3(b), the voltage was holding at 0.005 V for several hours to complete the lithiation process. This is why the charge of a lithium-ion cell comes to stop when the voltage reaches the threshold (e.g. around 4.2 V) and the current drops to a certain level during the constant voltage holding.

Supplementary to the information learned from voltage profiles, differential volt-

age or differential capacity curves can provide direct evidence of the phase transformations in the electrodes. Therefore, these differential curves are very useful for identifying the failure mechanisms of electrodes. For example, the voltage profiles of two graphite/NMC111 full cells with different capacity ratios after eight cycles (the formation period) at a rate of C/10 are plotted in Figure 2.4(a). Capacity ratio R is defined as the ratio of graphite capacity to NMC111 capacity. These full cells with different capacity ratios mean one type of full cell (R=4.54) has a much higher graphite loading. Nevertheless, it is impossible to learn the states of charge of the graphite just by looking at the voltage profiles after 8 cycles. In Figure 2.4(b), we observe that for the full cell with R=1.18 there are three distinct peaks corresponding to various lithium-carbon phases with the maximum capacity of 260 mAh g^{-1}, while for the cell with a higher graphite loading there is only one peak showing the capacity is only 55 mAh g^{-1} [96]. Therefore, it is clear that from dV/dQ vs. Q curves the graphite particles in the full cell with R=4.54 experience less lithiation/delithiation, that is, less mechanical fatigue.

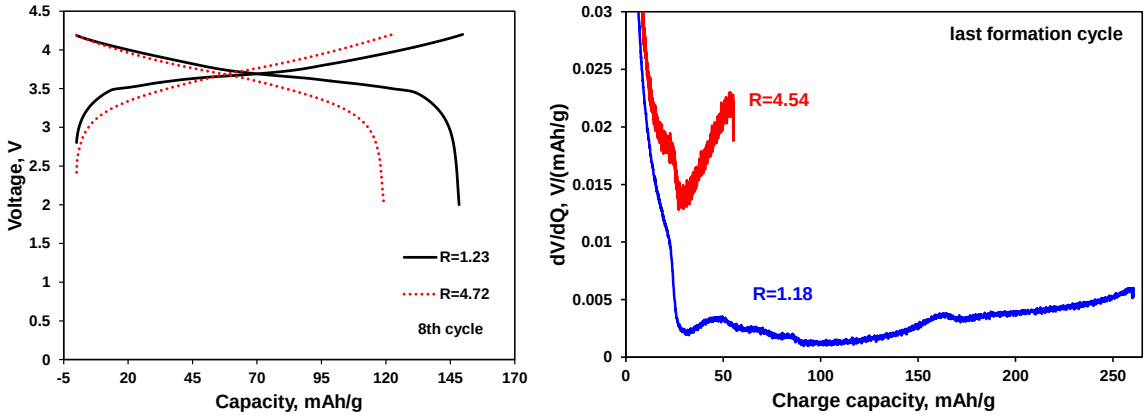

Figure 2.4: Voltage profiles (a) and the differential voltage curves (b) of two graphite-NMC111 full cells with different capacity ratios [96].

Another important approach to investigate the failure of batteries is to observe

the slippage of the charge/discharge capacity endpoints. For example, slippage of the charge/discharge capacity endpoints in a graphite/NMC111 full cell is shown in Figure 2.5. It is known that the parasitic reactions are the main cause of the failure of batteries. In general, these side reactions include lithium loss due to the SEI growth at the negative electrode, electrolyte oxidation at the positive electrode and lithium trap in the positive electrode [97]. As learned from ref [97], the displacement of charge and discharge capacity endpoints for any two cycles are denoted as Δ_C and Δ_D respectively. The mathematic relations are expressed as

$$\Delta_C = q_{ox} - 2q_p \tag{2.2}$$

$$\Delta_D = 2q_{Li} - q_{ox} \tag{2.3}$$

where q_{Li} is the lithium loss capacity due to the SEI formation, q_{ox} is the electrolyte oxidation capacity, and q_p is the lithium trap capacity at the positive electrode.

The Coulombic efficiency (CE) is defined as the ratio of discharge capacity to charge capacity. It can be expressed as

$$CE = 1 - \frac{\Delta_D}{Q_C} \tag{2.4}$$

where Q_C is the charge capacity of the cell in a cycle. Therefore the CE is only related with the slippage of the discharge capacity endpoints. CE is not 100% due to the side reactions. Furthermore, the capacity fade per cycle is determined by

$$\text{Capacity fade per cycle} = \Delta_D - \Delta_C \tag{2.5}$$

As long as the slippage rates of charge capacity endpoints and discharge capacity endpoints are different, there is a capacity drop at every cycle.

The charge/discharge capacity endpoints vs. time curves of two graphite/NMC111 full cells with different capacity ratios (different graphite loadings, but similar NMC111

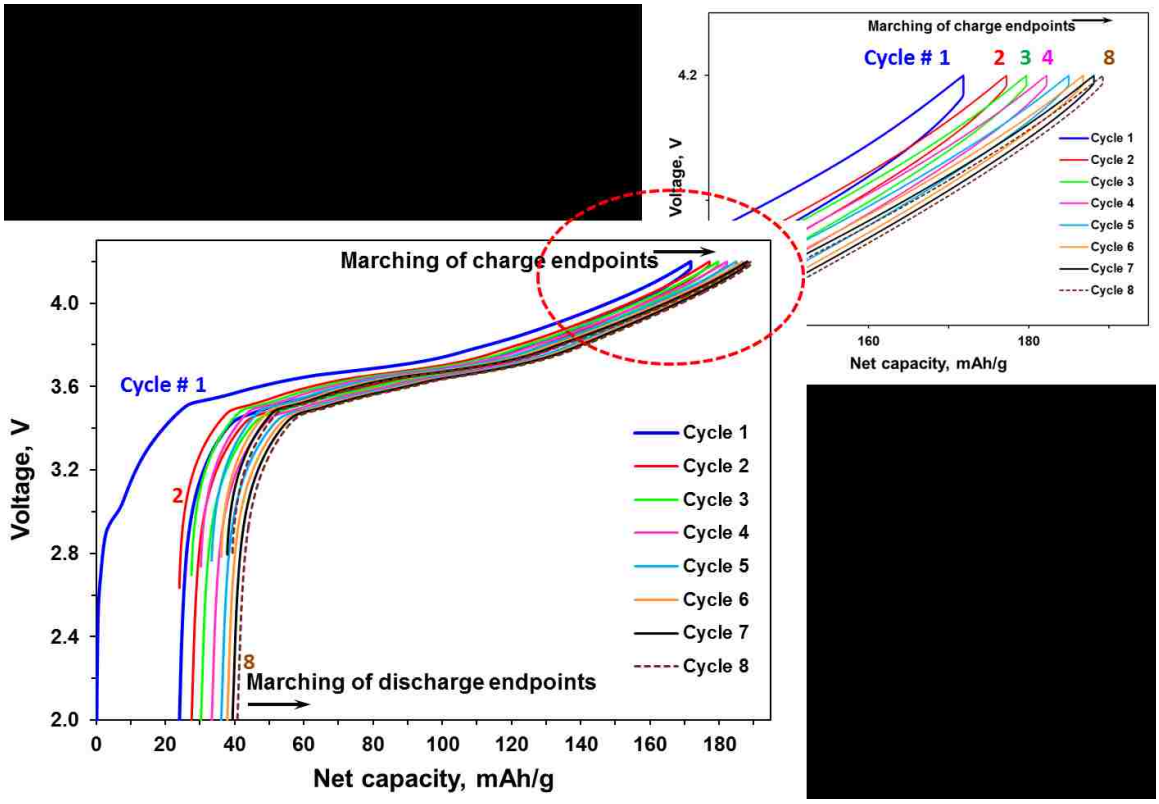

Figure 2.5: Slippage of the charge/discharge capacity endpoints in a graphite-NMC111 full cell [96].

loadings) as discussed earlier in Figure 2.4 are shown in Figure 2.6. The amount of the electrolyte oxidation reactions should only depend on the surface area or loading of the NMC111 electrode. Applying above equations to the curves in Figure 2.6, for the slippage of charge capacity endpoints, we obtain that the cell with a higher graphite loading (R=4.54) has a higher slippage rate of 0.4008 mA g^{-1} than the 0.0932 mA g^{-1} when R=1.18. The result suggests there is cross-talk between side reactions on the negative electrode and positive electrode [96][98].

For the slippage of discharge capacity endpoints, the cell with R=4.54 has a higher slippage rate of 0.4308 mA g^{-1} than the 0.1489 mA g^{-1} when R=1.18. This result can be understood as more graphite area is involved in the side reactions when R=4.54. The smaller difference between slippage rates of charge and discharge

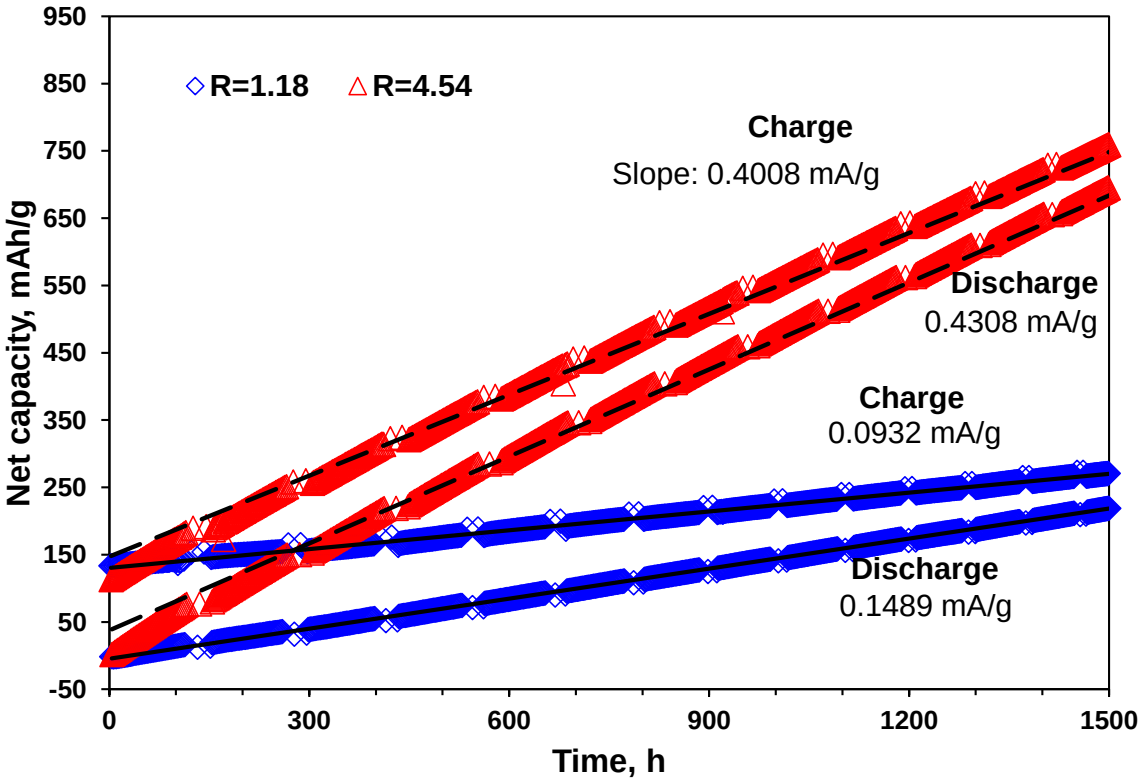

Figure 2.6: The charge/discharge capacity endpoints vs. time curves of two graphite-NMC111 full cells with different capacity ratios [96].

capacity endpoints for the cell with R=4.54 indicates the slower capacity fading rate.

2.2.2 Cyclic Voltammetry (CV)

CV is a widely used electroanalytical technique for rapidly acquiring qualitative information of the redox reactions, stability of reaction products, electrochemical irreversibility, heterogeneous electron transfer reactions and adsorption processes over a wide potential range. CV is consisted of linear scanning potential of the working electrode with a triangular waveform between initial and final potential limits. Cyclic voltammogram displayed as current (vertical axis) vs. potential (horizontal axis) is the current responses of the working electrode resulting from electrochemical reactions as a function of the applied potentials [99]. One advantage of CV is that data

processing is not necessary compared with plotting the differential capacity/voltage curves though these two approaches may give similar information.

At the interface between the electrode and liquid electrolyte, CV generally involves electrode reactions under kinetic control before reaching peak currents and under diffusion control after reaching peak currents. For highly reversible electrode reactions, the separation between peaks voltages and peak currents can be calculated from the mathematic equations [99]. For most electrochemical reactions, the electron transfer steps are often coupled with chemical reactions. CV can therefore be used to get qualitative information of reaction products and the reversibility of reactions by looking at the peaks voltages, peak currents and symmetry.

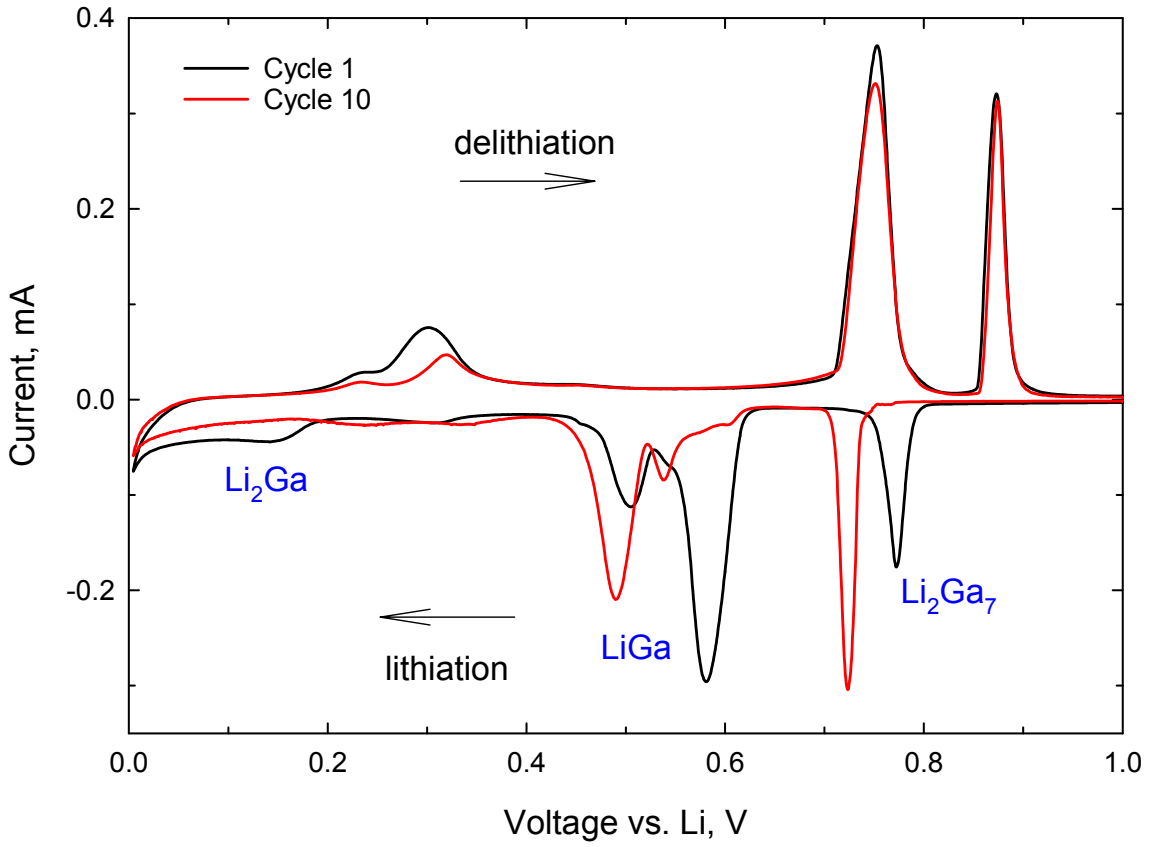

Figure 2.7: Cyclic voltammogram of the Ga thin film electrode with a voltage scan rate of 0.1 mV s^{-1} between 0.005-1.5 V.

For example, the cyclic voltammogram of the Ga thin film electrode is shown in

Figure 2.7. In the 1^{st} cycle, during lithiation (1.5→0.005 V) as lithium inserts into Ga, several Li-Ga phases start to form at the voltages around 0.8 V, 0.6 V and 0.1 V. These data are consistent with the results concluded from the voltage profiles [21]. After 10 cycles, we notice that the lithiation peak voltages are shifting to the left and peak currents are decreasing at low voltages. This observation clearly indicates the failure mechanisms of the Ga electrode, that is, the incomplete lithiation and lithium trap in Ga.

2.3 X-ray Photoelectron Spectroscopy (XPS)

XPS is heavily used to identify the elemental composition (except H and He) and corresponding chemical states on the shallow surface (10 nm) of solid materials [100]. The spectra are obtained after measuring the kinetic energy and number of the electrons escaped from the sample surface irradiated by focused beam of X-rays. The sample preparation is also very easy for XPS analysis.

In LIBs, XPS is widely used to study the composition of SEI layer, which is a very complicated mixture composed of both organic and inorganic species. It is confirmed that these inorganics species include LiF and Li_2CO_3. Since XPS can only detect the surfaces, depending on specific systems, argon ion etch may be beneficial for getting additional knowledge below the surfaces.

Chapter 3 Application of Nafion Binders in Silicon Negative Electrodes

Most of the content of this chapter is reproduced from the paper published as ref [135], that is, "J. Xu, Q. Zhang, Y.T. Cheng, High Capacity Silicon Electrodes with Nafion as Binders for Lithium-Ion Batteries, *J Electrochem Soc*, **163** (2016) A401-A405."

3.1 Introduction

There is an intense effort worldwide to develop new electrode materials for LIBs in order to satisfy future high power and energy density applications. Silicon can provide a theoretical capacity up to 3579 mAh g^{-1} (based on $Li_{15}Si_4$), which is about ten times higher than that of graphite electrode [101]. Resulting from large volume changes as lithium goes into and out of silicon, cracking and pulverization of silicon electrodes can cause the loss of electrical contact and new SEI formation on exposed surface, leading to rapid capacity fade. Novel binders and nanostructured silicon are two general approaches to improve the durability and performance of silicon electrodes.

For commercial LIBs, electrodes are composed of three essential components, which are active material, conductive additive and binder. The fundamental role of binder is to keep the electrode mechanically intact and adhered well to the current collector. Other ideal characteristics of binders include electrochemical stability over wide potential range, high melting point, low swelling rate in nonaqueous electrolyte, high lithium ionic conductivity, high electrical conductivity, capability to sustain volume change of active material particles, and good manufacturability [53][62][102]. Today, polyvinylidene fluoride (PVDF, monomer -CH_2-CF_2-) and styrene butadiene rubber (SBR) are commonly used as binders for graphite negative electrodes, and PVDF and polytetrafluoroethylene (PTFE, monomer -CF_2-CF_2-) can be used as binders for positive electrodes [53].

PVDF is known to perform poorly for high energy density electrode materials, such as silicon, because it fails to accommodate the large volume change during lithiation and delithiation [103][104]. Presently, there is much interest in developing effective binders for silicon-based electrodes. Crosslinked elastomeric polymer (PVDF + tetra-fluoroethylene + propylene) was shown to maintain good capacity retention for amorphous Si-Sn electrodes in spite of 125% volume change [58]. Carboxymethyl cellulose (CMC) and SBR were widely studied to improve the cycle life of silicon-based electrodes [59][105]-[109]. Polyfluorene based conductive polymer without adding conductive carbon black was shown to accommodate the volume change of silicon, and high capacity and long term cycling were achieved simultaneously [61]. Magasinski and coworkers first reported the use of polyacrylic acid (PAA) as a binder, which shows low swellability in carbonate electrolyte and high elastic modulus. The high concentration of carboxylic groups in PAA was attributed to the good electrochemical performance [104]. Similar to CMC and PAA, some polysaccharides extracted from natural products were demonstrated as binders for silicon nanoparticles with stable cycling behavior [110][111].

Lithium ion-exchanged Nafion (designated as Li-Nafion) has been reported as a binder to improve the cycling performance of micro-sized crystalline silicon powders (particle size, 44 μm) [60]. Sulfur-carbon electrode coated with Nafion was also demonstrated to improve the performance of lithium sulfur batteries [112]. Moreover, Nafion has been used in large scale applications as membranes in fuel cells because of its high protonic conductivity due to the sulfonic acid group ($-SO_3H^+$). After ion exchange in LiOH solution, Nafion becomes Li^+ conductive, which therefore has been considered as a candidate material for separator or electrolyte in lithium batteries [102][113]-[115].

Inspired by previous findings, we, in this chapter, investigated the electrochemical performance of silicon nanoparticles mixed with either Nafion or PVDF as a binder.

Ion-exchanged Nafion was also studied as a binder to compare with pure Nafion binder by replacing protons with Li^+. Unlike the rapid capacity fade of silicon electrodes with PVDF as a binder, we found that Nafion and ion-exchanged Nafion were both able to deliver specific capacity of silicon electrode more than 2000 mAh g^{-1} after 100 cycles with a high Coulombic efficiency. The specific capacity of silicon nanoparticles secured by Nation binders is comparable to that of nanostructured silicon electrodes, e.g., nanowires [62][110][116]. In addition, both rate capability test and long term cycling test show ion-exchanged Nafion can yield better performance of silicon electrode compared with Nafion.

3.2 Experimental

3.2.1 Electrode Preparation

Electrodes are composed of 50 wt% silicon powder (size 30-50 nm, Nanostructured & Amorphous Materials), 25 wt% conductive carbon black (Super P C65, TIMCAL) and 25 wt% binder. Binders used in our work include PVDF (Alfa Aesar), Nafion solution (D-520, Alfa Aesar) and ion-exchanged Nafion. The ion-exchanged Nafion solution was prepared in a customized titration set-up operated at room temperature. A 0.01 M LiOH (Sigma-Aldrich) aqueous solution was used as the titrant. The density of the Nafion solution is 0.93 g mL^{-1}, and the ion exchange capacity is typically 1.03 to 1.12 meq g^{-1}. For 1 mL of Nafion solution, it takes about 5 mL of LiOH aqueous solution to complete the ion exchange process. The N-methyl-2-pyrrolidone (NMP, 99.5%, Alfa Aesar) solvent was used to dissolve PVDF. Uniform slurries were obtained by mixing powders in a small sample vial immersed in an ultrasonic bath for 30 minutes. Finally, the slurry was cast onto a battery grade Cu foil (thickness, 12 μm) with a 127 μm doctor blade.

3.2.2 Electrochemical Measurement

Electrodes with diameter of 10 mm were punched from dried uniform laminates, and then were further dried at 130 °C for 12 hours in a vacuum oven. The silicon and lithium (0.38 mm thick, Sigma-Aldrich) disks were assembled as the positive and negative electrodes in CR2025 type coin cells in an argon-filled glove box (< 0.1 ppm of both oxygen and moisture, MBRAUN). One piece of microporous polypropylene film, Celgard 3501, was used as the separator in each cell. The electrolyte is 1M $LiPF_6$ salt in a mixture of ethylene carbonate and diethyl carbonate (EC:DEC=1:1 vol%, BASF). For comparison, the same electrolyte is prepared with an additive of 10 wt% fluoroethylene carbonate (FEC, BASF). Unless otherwise mentioned in this chapter, testing was carried out in coin cells without the FEC additive in the electrolyte. Cycling tests (discharge/charge curves, C-rate is expressed as C/R, for example, C/10 means 10 hours are required to completely discharge/charge) and rate capability tests were conducted under galvanostatic mode using two Bio-Logic potentiostats (MPG-2 and VMP-3) at room temperature. The theoretical capacity of 3600 mAh g^{-1} for silicon was used to calculate discharge/charge currents. CV was taken using Bio-Logic potentiostats (MPG-2 and VMP-3) between 1.0 V and 0.01 V with a potential scanning rate of 0.1 mV s^{-1}.

3.2.3 XPS and SEM Measurement

XPS (K-Alpha system, Thermo Scientific) was used to determine the chemical composition of pristine electrode and SEI layer on electrode surface after 10 cycles at the C/10 rate. For XPS measurements, post-cycling electrodes were obtained by disassembling the coin cells inside an argon-filled glove box and then washed thoroughly with the dimethyl carbonate (DMC, BASF) solvent and dried inside the argon-filled glove box. They were then transferred to the XPS analysis chamber without exposing to air using a Vacuum Transfer Module (Thermo Scientific).

Most SEM images were collected from a Hitachi S-4300 microscope (cold-cathode field emission), while others were collected from a FEI Quanta 250 microscope. Sample electrodes were obtained by disassembling the coin cells inside an argon-filled glove box and then washed thoroughly with the DMC solvent and dried.

3.3 Results and Discussion

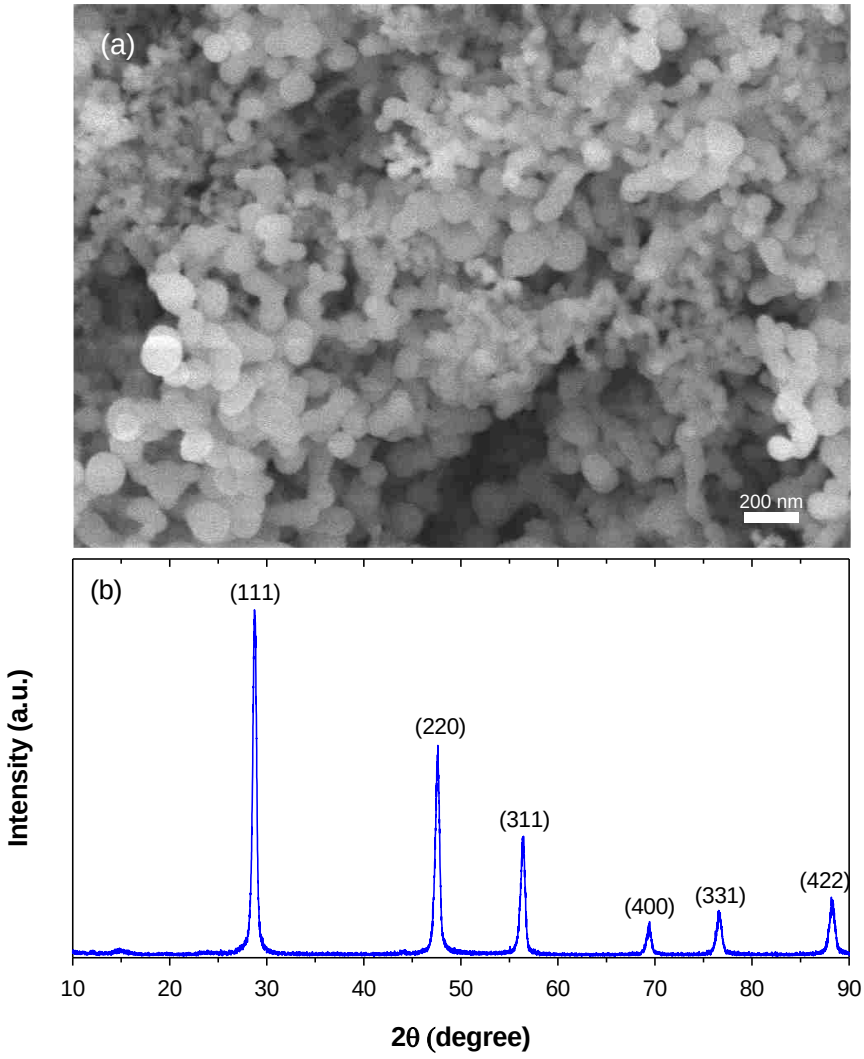

Figure 3.1: SEM image (a) and XRD pattern (b) of silicon nanoparticles.

The silicon nanoparticles used in my work are of spherical shape with an average diameter between 30 and 50 nm, as shown in Figure 3.1(a). The advantages of silicon

nanoparticles are the higher packing density compared with nanotubes or nanowires and the stable cycling behavior compared with micro-sized silicon. Large surface area of nano-sized silicon will enhance the rate performance as well as increase the amount of the side reactions. XRD (Siemens D5000, Cu $K\alpha$ radiation, λ= 0.154 nm, 40 kV, 30 mA, 0.01 °/step) pattern in Figure 3.1(b) confirms the pristine silicon is crystalline, though it will become amorphous during alloying with lithium.

3.3.1 CV and Cycling Performance

The electrochemical characteristics of silicon electrodes with different binders were first examined by cyclic voltammetry between 1.0 V and 0.01 V at a relatively slow potential scanning rate of 0.1 mV s^{-1}. The cyclic voltammograms for the first two cycles are shown in Figure 3.2. In the 1^{st} cycle, no obvious peaks were present during lithiation as the crystalline silicon was transformed to an amorphous Li-Si alloy. Because the potential reached 10 mV, the high lithium concentration $Li_{15}Si_4$ phase with a theoretical capacity of 3579 mAh g^{-1} was formed [101][117]. The cross over between lithiation and delithiation curve in the 1^{st} cycle around 0.1 V could be attributed to continuous SEI formation [118].

During delithiation, two types of amorphous silicon phases (a-Li_xSi) formed as indicated by the respective peaks around 0.3 V and 0.5 V, though the detailed mechanism of forming these two amorphous phases was unknown [35][110][117][118]. In the 2^{nd} cycle, the peaks around 0.2 V and 0.01 V were attributed to lithium alloying with amorphous silicon, and the delithiation peaks were around 0.3 V and 0.5 V. For all the electrodes, delithiation peaks shifted to the right as the electrodes were cycled. This increase in the overpotential was due to continuous SEI formation on the electrode surface, causing increasing impedance.

In order to know more about the electrochemical performance of silicon electrode mixed with different binders, these electrodes were cycled between 1.0 V and 0.01 V

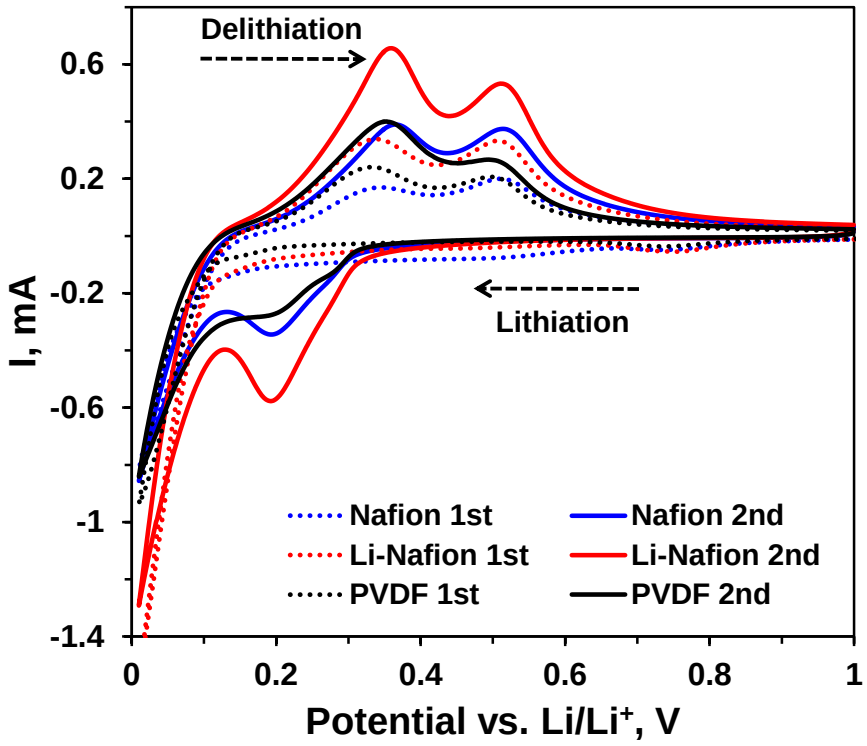

Figure 3.2: Cyclic voltammograms of silicon electrodes with various binders. The voltage limits are 1.0 V and 0.01 V, and the potential scanning rate is 0.1 mV s^{-1}.

under constant current at room temperature. The amount of silicon was about 0.4 mg cm^{-2} for all sample electrodes. The initial discharge/charge voltage vs. capacity curve is shown in Figure 3.3(a). For crystalline silicon electrodes, amorphization always happens during the first cycle as indicated by the plateau in the discharge curve as seen in Figure 3.3(a). These voltage profiles are very similar to those reported in the literature [62][104][110].

The specific capacity and Coulombic efficiency vs. cycle number curves for electrodes with different binders and electrolytes are shown in Figure 3.3(b). The capacity of silicon electrode with PVDF binder degraded drastically after the 1^{st} cycle. In contrast, the capacity retention of silicon electrodes using pure or ion-exchanged Nafion as binders is much improved. In the absence of FEC in the electrolyte, the initial capacity based on pure silicon mass was 3466, 3956 and 4342 mAh g^{-1}, for electrodes containing PVDF, Nafion and ion-exchanged Nafion, respectively. Since the specific

capacity was calculated using the measured silicon mass in each electrode, the value of specific capacity may have error depending on the accuracy of silicon mass measurement. This may explain why the specific capacity of 4342 mAh g^{-1} is larger than the theoretical capacity of 4200 mAh g^{-1} for the most saturated phase $Li_{22}Si_5$.

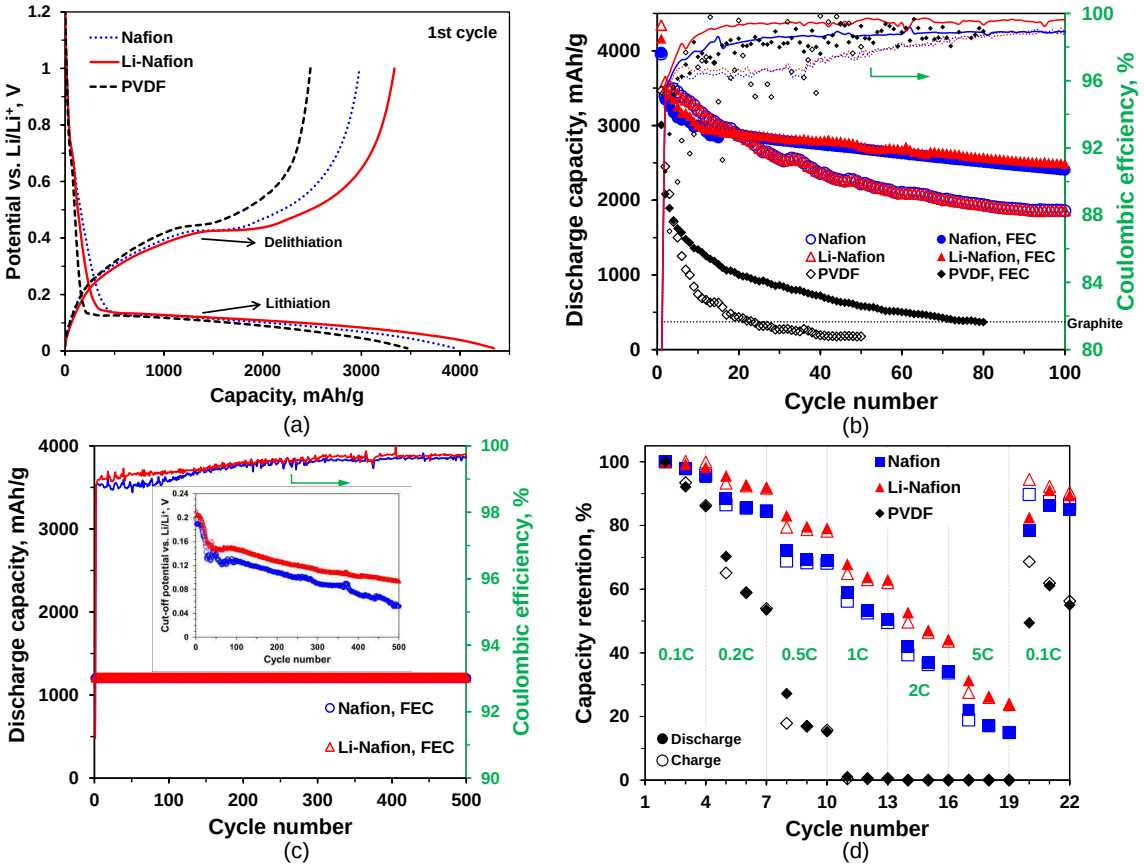

Figure 3.3: Electrochemical characteristics of silicon electrodes containing different binders, and the testing potential window was from 0.01 V to 1.0 V vs. Li/Li^+, (a) Initial discharge/charge voltage profile cycled at C/10. (b) Discharge capacity and Coulombic efficiency vs. cycle number tested at C/10, curves with filled markers and solid lines are for electrodes with FEC in the electrolyte and curves with empty markers and dotted lines are for electrodes without FEC in the electrolyte. (c) Discharge capacity and lithiation cut-off potential vs. cycle number for electrodes with Nafion as binders in the presence of FEC in the electrolyte tested at 1C with a capacity limit of 1200 mAh g^{-1}. (d) Normalized discharge/charge capacity retention at different current densities, 1C = 3600 mA g^{-1}, filled marker indicates discharge process and empty marker indicates charge process.

The Coulombic efficiency is an important indicator for the cycling stability of

electrodes. From Figure 3.3(b), the Coulombic efficiency in the 1^{st} cycle was 72%, 75% and 77% for silicon electrodes with PVDF, Nafion and ion-exchanged Nafion as binders, respectively. The initial low Coulombic efficiency was due to the irreversible Li loss caused by the formation of SEI. An increase in the Coulombic efficiency after the 1^{st} cycle suggests that most SEI formed during the first discharge process. As a result of large volume changes upon cycling, the loss of active silicon particles and a continuous growth of SEI on freshly exposed silicon surface were believed to be the cause of low Coulombic efficiency and irreversible capacity loss.

FEC was reported to yield stable cycling of silicon electrodes by forming stable and unique SEI film protecting silicon against oxidation and electrolyte from decomposition [119][120]. In Figure 3.3(b), higher capacity retention (with filled markers) and higher Coulombic efficiency (in solid lines) of silicon electrodes with Nafion binders were obtained using the electrolyte with the FEC additive. Moreover, Figure 3.3(c) shows the stable cycling of silicon nanoparticles mixed with Nafion binders for 500 cycles at a rate of 1C with a lithiation capacity limit of 1200 mAh g^{-1}. The morphology and continuous formation of SEI during long term cycling for silicon electrode mixed with Nafion and ion-exchanged Nafion could be different and this would lead to the difference of both impedance rise of the cell and state of charge of active silicon nanoparticles. Indeed, lithiation cut-off potential vs. cycle number curve in Figure 3.3(c) indicates that silicon/ion-exchanged Nafion cell behaves better due to the higher cut-off potentials, suggesting the lower impedance and longer cycle life of the cell. The cyclic test results based on Nafion and ion-exchanged Nafion binders are quite comparable with that of sodium alginate and are better than that of CMC, which are widely studied binders in recent years [110].

Figure 3.3(d) compares the discharge/charge capacity retention at different current densities for silicon electrodes mixed with different binders at room temperature normalized based on the data from the 2^{nd} cycle. The theoretical capacity 3600 mAh

g^{-1} for silicon was used to calculate discharge/charge currents, thus current density for 1C was 3600 mA g^{-1} for all the electrodes. Since the performance of Si/PVDF was very poor at C/10, its capacity retention was, unsurprisingly, close to zero at 1C, 2C and 5C. We suggest that PVDF around silicon particles cannot effectively guarantee fast lithium ion transport and thus lithiation and delithiation were incomplete at high current densities. On the other hand, silicon electrodes with Nafion and ion-exchanged Nafion as binders were still cycleable at 1C, 2C, and 5C. Furthermore, the ion-exchanged Nafion yielded even better rate performance compared with pure Nafion as seen in Figure 3.3(d) which is likely due to its superior capability to provide lithium transport paths to silicon nanoparticles.

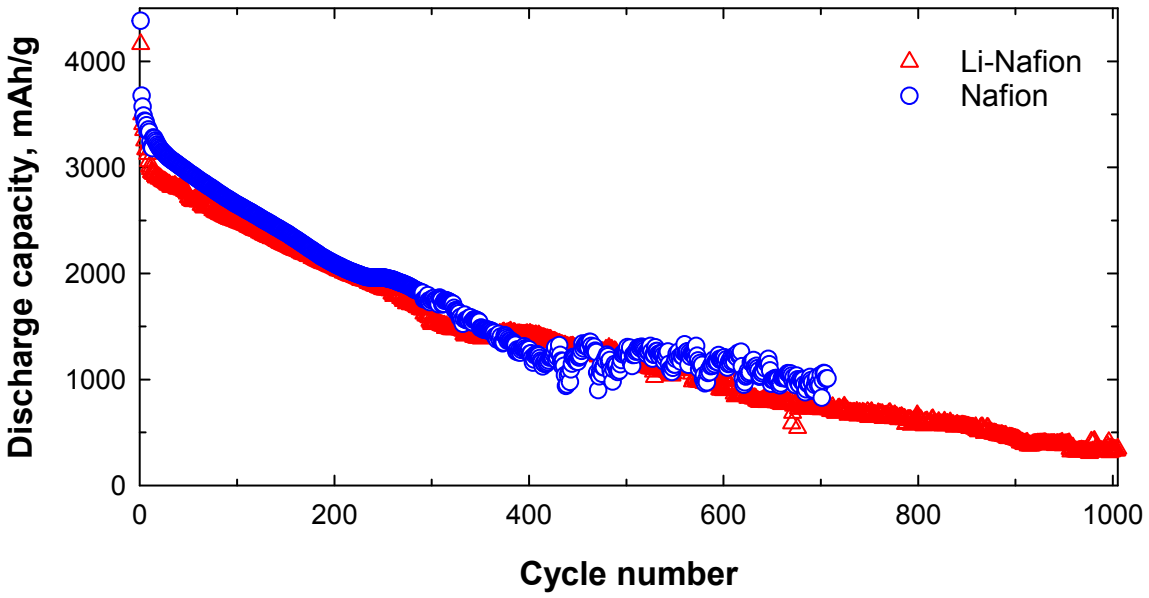

Figure 3.4: Long term cycling performance of the Si/Nafion and Si/Li-Nafion electrodes. Electrodes were cycled at C/10 between 0.01-1.0 V.

Figure 3.4 shows the long term cycling performance of the Si/Nafion and Si/Li-Nafion electrodes after 700 and 1000 cycles respectively. Electrodes were cycled at C/10 between 0.01-1.0 V and FEC was present in the electrolyte. The Si/Li-Nafion electrode in Figures 3.3 and 3.4 are the same, while the Si/Nafion electrodes are from

the same batch of electrode laminate. Similar to the degradation trend in Figure 3.3, there is no sudden capacity drop as expected due to the continuous loss of lithium and active silicon. After 400 cycles, the Si/Nafion system became unstable as the capacity was fluctuating. The reason for this phenomenon was unclear.

3.3.2 Electrode Surface Morphology

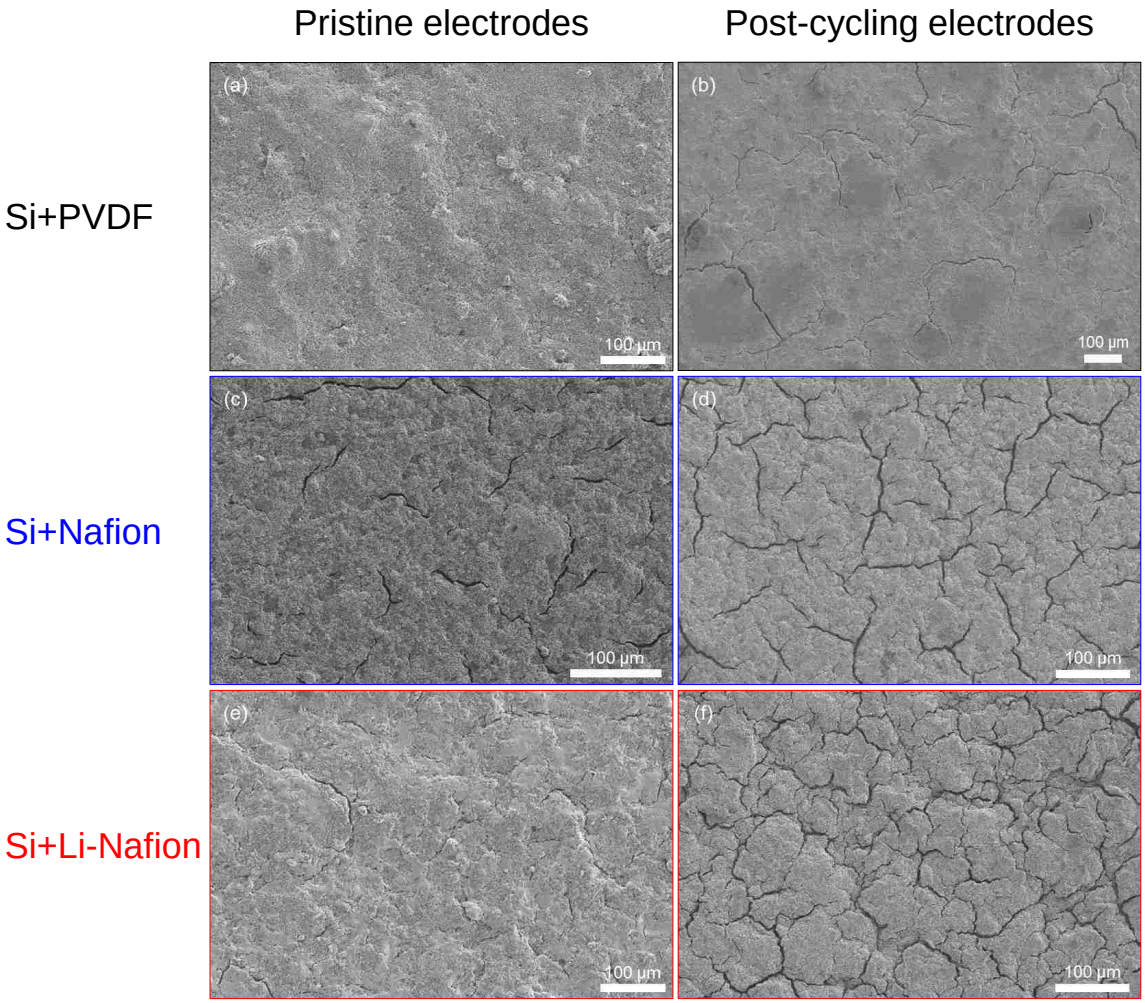

Figure 3.5: SEM images of pristine electrodes and post-cycling electrodes (without FEC) containing three different binders, (a,b) PVDF, (c,d) Nafion, and (e,f) Li-Nafion. Electrodes were cycled at C/10 for 10 cycles between 0.01-1.0 V.

Corresponding to the electrochemical performance in Figure 3.3, the FEC-free

electrodes tested for 10 cycles at C/10 between 0.01-1.0 V were opened to examine the surfaces. A comparison between the pristine electrodes and post-cycling electrodes is shown in Figure 3.5. Large and small cracks are visible in all three types of electrodes due to the expansion and contraction of silicon particles. It seems the Si/PVDF electrode has less cracks, which suggests the good binding capability of PVDF. Nevertheless, we believe the Nafion binders can be beneficial for the capacity retention by providing lithium transport to isolated silicon nanoparticles.

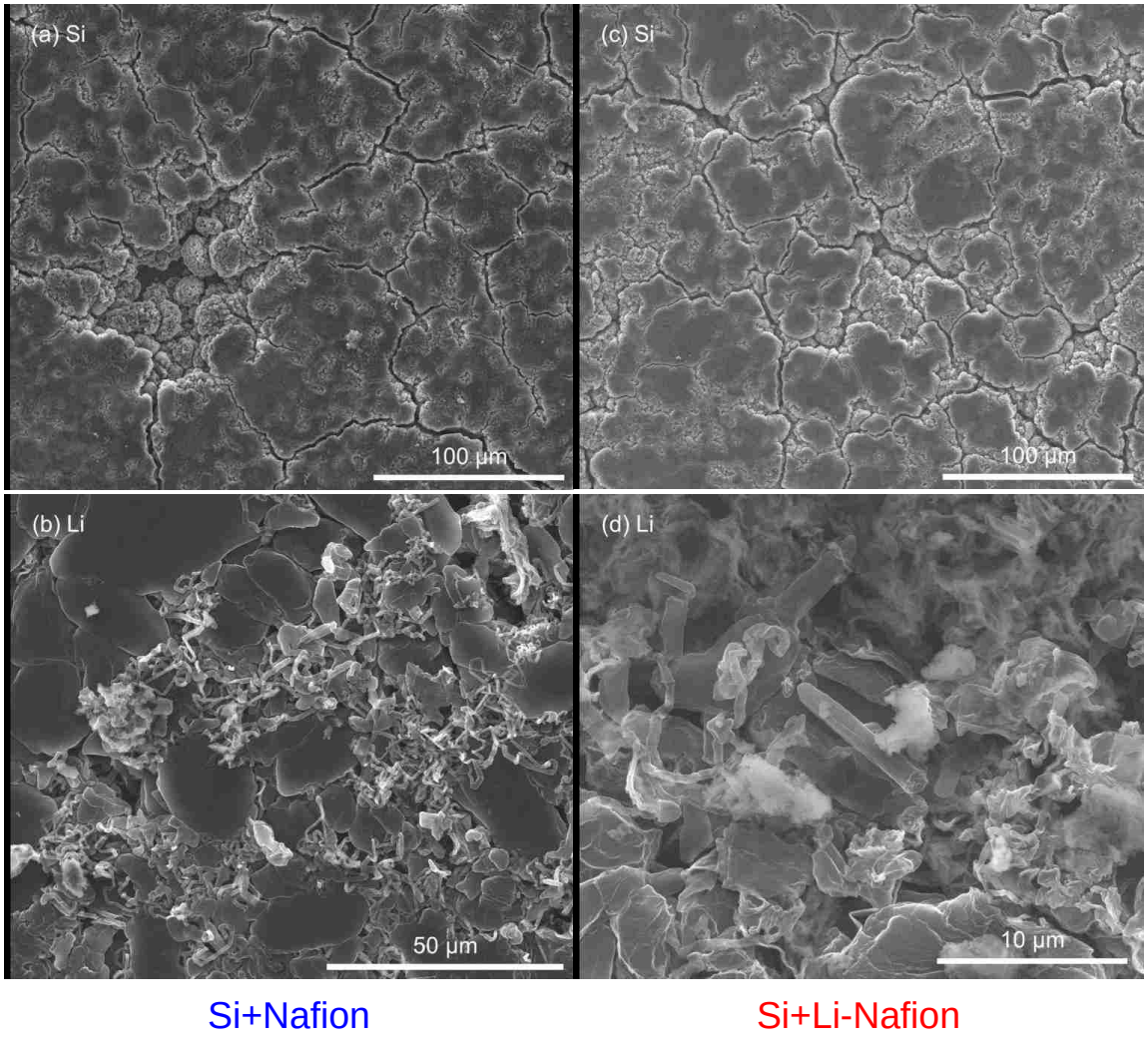

Figure 3.6: SEM images (taken from a FEI Quanta 250 microscope) of silicon and lithium from Si/Nafion (a,b) and Si/Li-Nafion (c,d) electrodes after long term cycling. Electrodes were cycled at C/10 between 0.01-1.0 V.

Corresponding to the electrochemical performance in Figure 3.4, Figure 3.6 shows the SEM images of silicon and lithium from Si/Nafion and Si/Li-Nafion electrodes tested with FEC in the electrolyte for more than 700 cycles at C/10 between 0.01-1.0 V. The silicon surfaces are overall smooth, however, the disintegration of electrodes is apparent below the surface as learned from Figure 3.6(a). This observation indicates isolated silicon nanoparticles most probably cannot participant in electrochemical reactions anymore, resulting in permanent capacity loss. On the other hand, from Figure 3.6(b,d), on the lithium foil surfaces, there are a lot of needle-like dendrites formed on some locations. Based on our observation, the formation and growth of lithium dendrite are not predictable. The dendrite may penetrate the separator to short-circuit the cell. Herein, currently pure lithium has not been used as the negative electrode in LIBs.

3.3.3 XPS Spectra Analysis

XPS measurements were carried out to study the chemical composition of the surface of the electrodes before and after electrochemical cycling tests. Figure 3.7 shows C 1s, F 1s and Si 2p spectra for the fresh electrodes containing different binders, which were always stored inside an argon-filled glove box after fabrication. In Figure 3.7(a), the first C 1s peak at 284.5 eV is attributed to carbon black and C-C bonds in PVDF and Nafion binders. The second peak around 286 eV and the third peak at 290.4 eV are identified as C-H_2 bonds and C-F_2 bonds in PVDF, respectively. The last peak around 291.8 eV corresponds to CF_2/CF groups in Nafion and ion-exchanged Nafion [121]. From Figure 3.7(b), the first F 1s peak at 687.4 eV is assigned to CF groups in PVDF and the second peak at 688.8 eV is assigned to CF groups in Nafion and ion-exchanged Nafion [121]. In Figure 3.7(c), the first broad peak around 100 eV indicates the existence of silicon, and the second broad peak around 103.5 eV indicates the existence of silicon oxides on silicon surface [118]. We noticed that there

are more than one type of silicon oxides in the electrodes containing Nafion as shown in Figure 3.7(c) which may be due to the influence of the deionized water introduced during electrode fabrication.

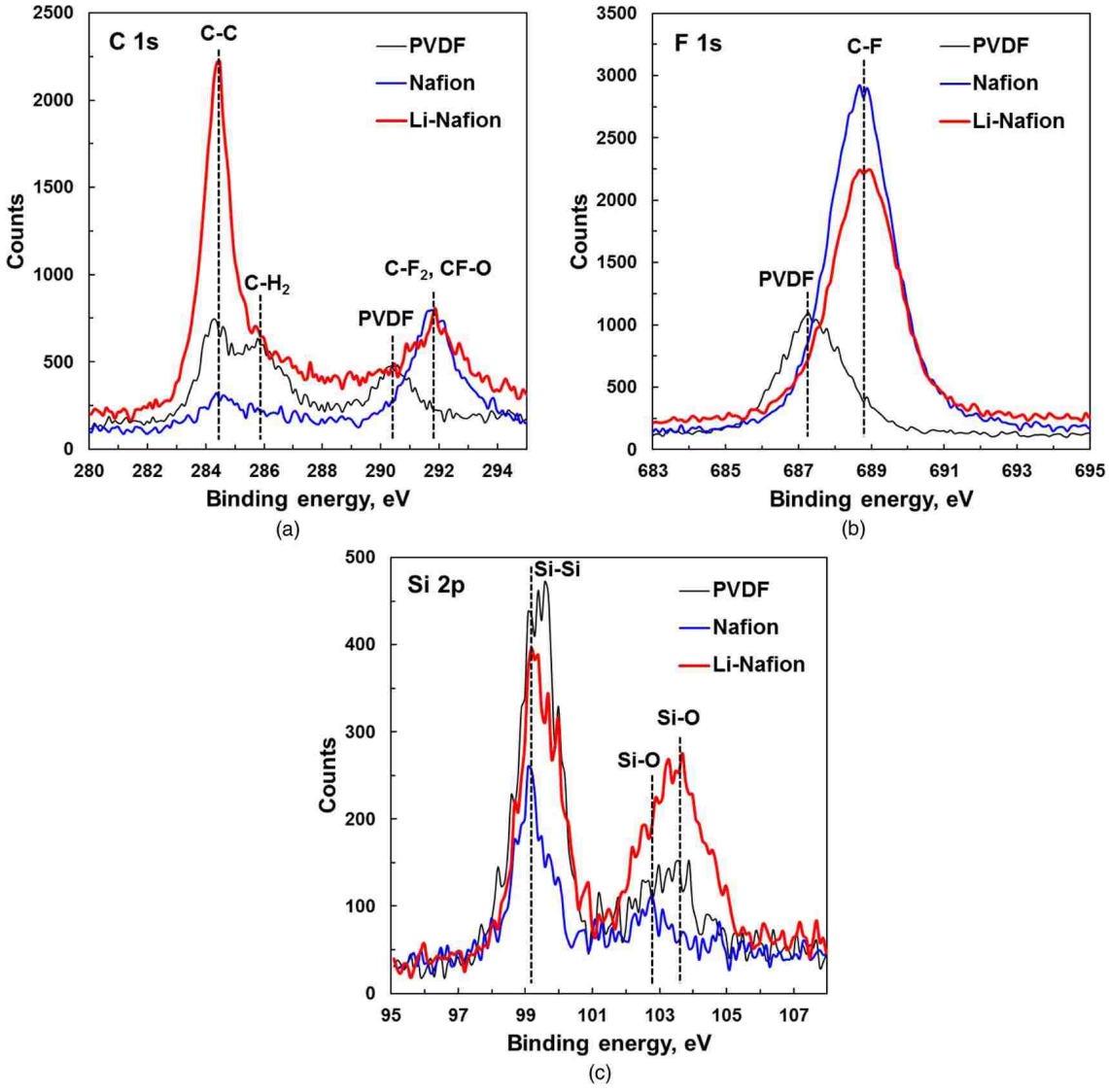

Figure 3.7: XPS spectra of pristine electrodes containing different binders, (a) C 1s peaks, (b) F 1s peaks and (c) Si 2p peaks.

XPS spectra (C 1s, O 1s, F 1s and Si 2p) for electrodes containing different binders after 10 discharge/charge cycles between 1.0 V and 0.01 V at C/10 are presented in Figure 3.8. No FEC was added when testing these electrodes. By the end of the

10^{th} charging process, all the electrodes were held at 1.0 V for 2 hours in order to complete delithiation. In Figure 3.8(a), the C-C peak, which is usually associated with carbon black and alkane species or surface hydrocarbon contamination, is absent for Nafion and ion-exchanged Nafion and it is also invisible for PVDF. Kovalenko and coworkers reported a similar result but this phenomenon is still very different from other reports [110][118][122]. The peak around 286.8 eV can be attributed to C-O bonds in carbonaceous solvent reduction products (for example, ethers ROLi, esters RCOOLi and alkyl carbonate solutions $ROCO_2Li$) and the peak at 288.5 eV can be attributed to O-C=O bond in alkyl carbonate solutions [122][123]. Moreover, the peak at 290 eV for Li_2CO_3 formation is not seen in the cases of these three binders. This is possibly due to the amount of formed Li_2CO_3 after 10 cycles is insufficient for XPS detection or Li_2CO_3 is very close to the silicon particle surface and is covered by other organic SEI components.

A single broad O 1s peak centered at around 533 eV is observed in Figure 3.8(b), which is likely caused by species containing C=O bonds at around 531.5 eV and C-O bonds at 533-534 eV and O-C=O bonds at around 534 eV [118]. In Figure 3.8(c), a dominant peak at around 687 eV indicates the formation of LiF and the peak at around 689 eV indicates the presence of $LiPF_6$ residue and its decomposed products $Li_xPF_yO_z$. Additionally, based on Figure 3.8(c), it seems that PVDF is favorable for formation of inorganic $Li_xPF_yO_z$ and unfavorable for LiF formation. Unlike fresh electrodes, no useful information can be extracted from the Si 2p spectra shown in Figure 3.8(d) because silicon particles are completely covered by SEI. The LiF has been widely accepted as a beneficial SEI component for improved cycling behavior, especially when FEC is used as the electrolyte additive [124][125]. By comparing with our FEC free case, we suggest that both Nafion and ion-exchanged Nafion have the capability of transporting lithium ions to silicon nanoparticles and thus maintaining relatively stable cycling performance as seen in Figure 3.3(b).

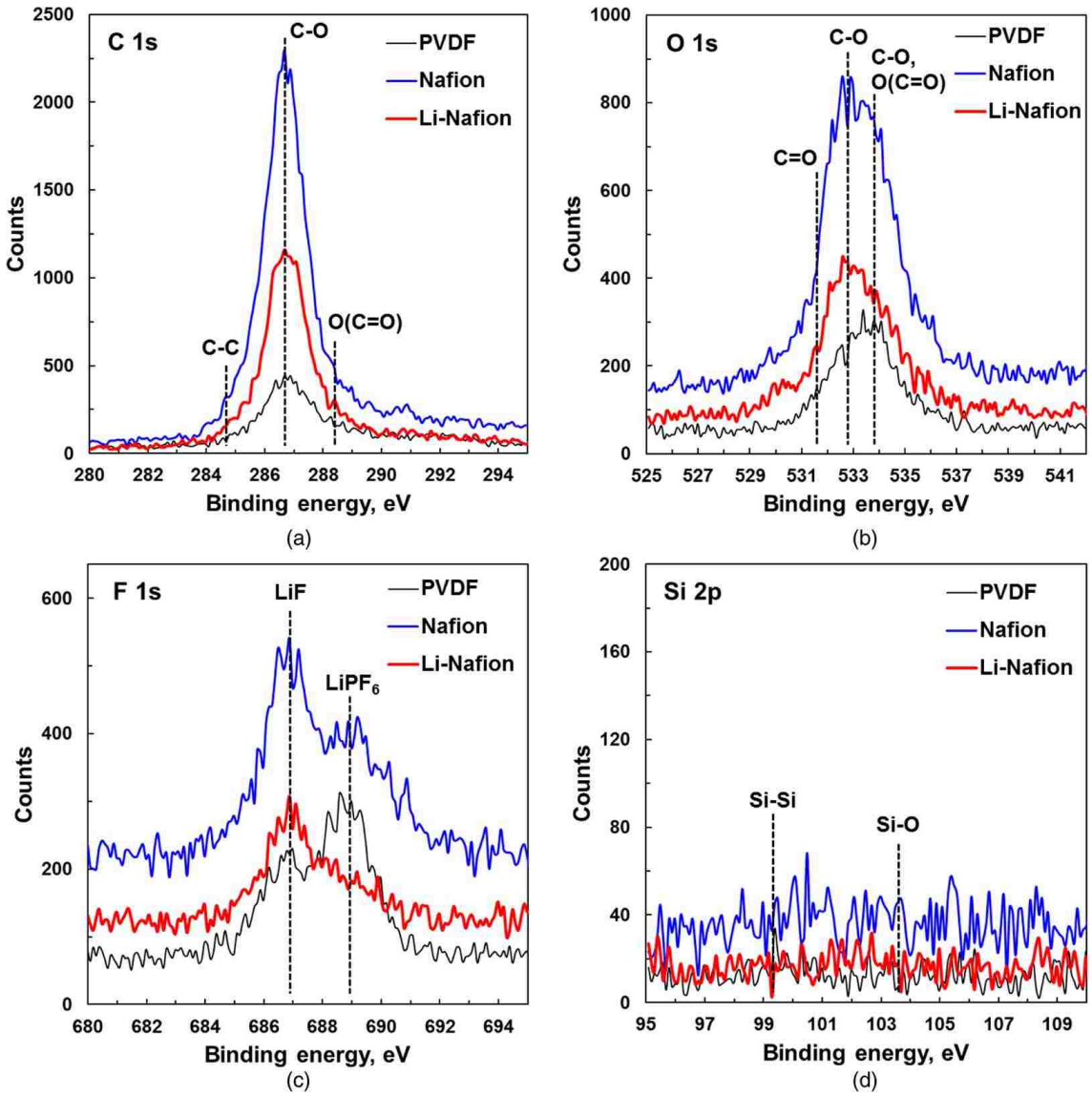

Figure 3.8: XPS spectra of electrodes containing different binders after 10 discharge and charge cycles at the C/10 rate, electrodes were holding at 1.0 V for 2 hours after 10th charge, (a) C 1s peaks, (b) O 1s peaks, (c) F 1s peaks and (d) Si 2p peaks.

Corresponding to the electrochemical performance in Figure 3.4 and SEM observation in Figure 3.6, only the XPS Si 2p spectra of the Si/Nafion and Si/Li-Nafion electrodes tested with FEC in the electrolyte for more than 700 cycles are plotted in Figure 3.9 because the spectra for other elements are very similar to those illustrated in Figure 3.8(a,b,c). The Si-O peak around 103 eV suggests the existence of silicon

oxides possibly coming from the original oxides on silicon particle or the reactions between silicon and electrolyte. The amount of reaction product Li_xSiO_y between silicon and electrolyte may become significant only after a long period of cycling [126].

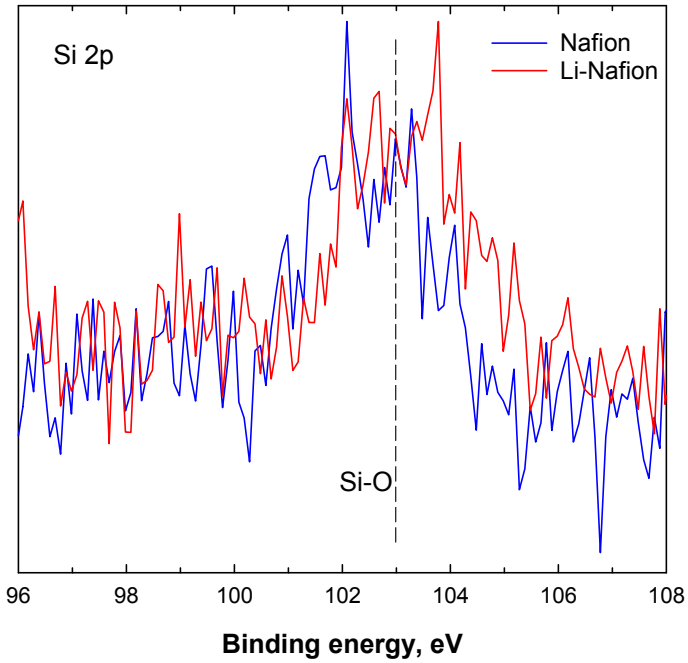

Figure 3.9: XPS Si 2p spectra of electrodes containing Nafion and Li-Nafion after long term cycling at C/10 between 0.01-1.0 V.

3.4 Summary

Ionic conducting polymers Nafion and ion-exchanged Nafion were shown to be promising binders for silicon electrodes in LIBs. For comparison, PVDF was shown to be unsuited for silicon electrodes because of the poor cycling behavior. For silicon nanoparticles, Nafion with or without ion exchange resulted in long cycling durability with a high capacity of more than 2000 mAh g^{-1} for 100 cycles at the C/10 current rate. It is also further confirmed that the better performance of silicon electrodes was achieved by adding a small amount of FEC to the electrolyte. Nafion binders were believed to be capable of transporting lithium ions and forming ionic conductive films

between the liquid electrolyte and silicon particles. This work not only demonstrates Nafion as promising binders for silicon electrodes but also inspires more efforts to better understand binding mechanisms.

Chapter 4 A Comparative Study of Polymeric Binders for Silicon Electrodes in Lithium-Ion Full Cells

4.1 Introduction

Research and development of LIBs to satisfy future high power and high energy applications, for example, hybrid electric and pure electric vehicles, is attracting a worldwide effort. Silicon is considered one of the most promising negative electrode materials as it is capable of delivering a very high theoretical specific capacity of 3579 mAh g^{-1} (based on $Li_{15}Si_4$), comparing to 372 mAh g^{-1} of the state-of-the-art graphite based negative electrodes [101]. However, the major obstacle to commercialize silicon electrode is its poor cycling behavior resulted from the large volume changes associated with Li-Si reactions. Specifically, both chemical degradation, caused by the unstable SEI formation and growth, and mechanical degradation, caused by the cracking of electrode and SEI, contribute to the rapid failure of silicon electrodes [96][127].

Many approaches have been taken to address the problem of large volume changes and to improve the performance of silicon electrodes, for example, different forms of nanostructured silicon [39][128], Si/C composite [108][129][130], and electrolyte additives [119][120][131]. Alternatively, polymeric binders, an essential component of the silicon electrode, have been widely studied, including green and natural binders and conductive binders, such as carboxymethyl cellulose (CMC), polyacrylic acid (PAA), and alginate [60][104],[109]-[111],[132]-[134]. In general, several key characteristics of binders for silicon are believed desirable: (1) electrochemical stability, (2) binding capability, and (3) ability to accommodate the volume changes during charge/discharge [62][103][134].

Lithium-ion half cell using silicon as the working electrode and pure lithium as the

counter/reference electrode is the most common configuration of studies in published reports. Although promising performance of silicon electrodes has been achieved in Si vs. Li half cells, these cells are not practical systems. Moreover, the failure mechanism of the silicon electrode in full cells may be different from that in half cells, because of the limited lithium supply by the positive electrode and parasitic reactions happening on both negative and positive electrodes. Recently, we demonstrated that Nafion and Li-Nafion were promising binders for nanoparticle silicon electrodes [135]. Here, we report the full cell studies of the electrochemical behavior of silicon nanoparticles mixed with Nafion in Si/$LiNi_{1/3}Mn_{1/3}Co_{1/3}O_2$ (NMC) coin cells. The results will be compared with that using either sodium alginate or PVDF as binders. Sodium alginate is chosen because it represents a family of binders with rich carboxylic acid groups (CMC, PAA) and its good cycling behavior in half cells was reported recently [110]. This work shows that silicon electrodes using either Li-Nafion or sodium alginate as binders can be cycled in full cells for more than 100 cycles at C/1 and 1200 mAh g^{-1} capacity. Deep charge/discharge testing shows that higher capacity retention rates are achieved in the Si/Li-Nafion and Si/sodium alginate systems. Failure analysis of these full cells is conducted using various material and electrochemical characterization techniques.

4.2 Experimental

4.2.1 Electrode Preparation

Negative electrodes were made of 50 wt% silicon powder (particle diameter 30-50 nm, Nanostructured & Amorphous Materials), 25 wt% conductive carbon black (Super P C65, TIMCAL), and 25 wt% binder, including PVDF (Alfa Aesar), sodium alginate (Sigma-Aldrich), Nafion solution (D-520, Alfa Aesar) and ion-exchanged Nafion. The ion-exchanged Nafion solution was prepared at room temperature using 0.01 M LiOH (Sigma-Aldrich) aqueous solution as the titrant. The N-methyl-2-pyrrolidone (NMP,

99.5%, Alfa Aesar) and deionized water were used as solvents to dissolve PVDF and sodium alginate, respectively. Uniform slurries were obtained after sonication for 30 minutes. Finally, the slurry was casted onto a 12 μm thick battery grade copper foil with a 127 μm doctor blade (Hohsen, Japan). The final thickness of the silicon electrode is about 20 μm, excluding copper foil and the mass loading of silicon is about 0.4 mg cm^{-2}.

Positive electrodes were made of 92 wt% NMC (Umicore), 4 wt% conductive carbon black (Super P C65, TIMCAL), and 4 wt% PVDF (No.1100, Kureha, Japan). Firstly, carbon black and PVDF solution in NMP were well mixed in a planetary mixer/deaerator (Kurabo Mazerustar KK-250S, Japan). Secondly, NMC was added to the slurry, and a homogeneous slurry was obtained after mixing for 1 hour using a homogenizer (Polytron PT10-35) at 4000 rpm. Finally, the slurry was spread onto a 15 μm thick aluminum foil using an automatic coater (MTI Corp.) with a blade gap of 200 μm. After drying at ambient temperature, the NMC laminate was calendered to about 32% porosity using a rolling press (MTI Corp.). The thickness of the NMC electrode excluding aluminum foil is about 66 μm and the mass loading of NMC is about 14 mg cm^{-2}.

Silicon electrodes with diameter of 14 mm and NMC electrodes with diameter of 12 mm were punched from dried uniform laminates, followed by drying at 110 °C overnight in a vacuum oven. The electrodes then were transferred into an argon-filled glove box for coin cell fabrication. The Si:NMC capacity (in mAh) ratio in full cells is close to 0.8:1. The excess capacity of NMC electrode is necessary considering significant SEI formation on the Si electrode during the first few cycles.

4.2.2 Coin Cell Assembly and Electrochemical Measurement

The NMC and silicon disks were assembled as the positive and negative electrodes in CR2025 type coin cells in an argon-filled glove box ($<$ 0.1 ppm of both oxygen and

moisture, MBRAUN), using one piece of microporous polypropylene film (Celgard 2400) as the separator and 55 μL electrolyte in each cell. The electrolyte is 1M $LiPF_6$ salt in a mixture of ethylene carbonate and diethyl carbonate (EC:DEC=1:1 vol%, BASF) with an additive of 10 wt% fluoroethylene carbonate (FEC, BASF). Coin cells were sealed by an automatic crimper (Hohsen, Japan).

Cycling tests were conducted under galvanostatic mode using two Bio-Logic potentiostats (MPG-2 and VMP-3) and a cycler (BCS-805) at ambient temperature. The theoretical capacity of 3600 mAh g^{-1} for silicon was used to calculate charge/discharge currents. In this chapter, charge means lithium atoms leaving the NMC electrode to react with silicon, and discharge is the reverse process. The Coulombic efficiency is defined as the ratio of discharge capacity to charge capacity.

4.2.3 Silicon Surface Characterization

After cycling tests, coin cells were held at 2.8 V for 2 hours and then opened by a manual disassembler (Hohsen, Japan) inside the glove box. Silicon electrodes were washed thoroughly with dimethyl carbonate (DMC, BASF) solvent and dried. SEM images were collected from a Hitachi S-4300 microscope (cold-cathode field emission). XPS was used to determine the chemical composition of SEI layer on electrode surface after 100 cycles at the C/1 rate. Depth profiles of electrodes were obtained by XPS measurements after a short period of ion gun etching (the ion gun energy is 2 keV and each etch step lasts for 4 s). To avoid air exposure, a Vacuum Transfer Module (Thermo Scientific) was used to transfer electrodes from the glove box to the XPS analysis chamber.

4.2.4 Nanoindentation Measurement

For nanoindentation measurements, sodium alginate and PVDF films were prepared by drop coating, while Nafion membrane is commercially available (NR-212, Ion

Powder Inc.). Nanoindentation test was conducted on a G200 nanoindenter (Agilent Tech.) with a Berkovich tip using the continuous stiffness measurement mode.

4.3 Cycling Performance for the Partial Charge/Discharge Test

Silicon/NMC full cells were cycled at C/10 (corresponds to 360 mA g^{-1}) for the first 2 cycles to stabilize the system and cycled at C/1 with a specific charge capacity of 1200 mAh g^{-1} (based on silicon mass) for 100 cycles in a voltage range of 4.2-2.8 V. This is called partial charge/discharge cycling in this chapter and its behavior is presented in Figure 4.1. Constant charge capacity 1200 mAh g^{-1} is chosen for two reasons: (1) to study the roles of binders when the volume change of silicon particles is significantly reduced to about 100% compared with about 300% volume change associated with formation of the fully lithiated phase $Li_{15}Si_4$ [136]; (2) the demonstration of a high performance and durable 1200 mAh g^{-1} negative electrode would further stimulate research on high voltage and high capacity positive electrodes since increasing the capacity of the negative electrode alone has a negligible effect on the total capacity of 18650 Li-ion cells if the positive electrode capacity remains the same [30]. In the 1^{st} charge process, the crystalline silicon (XRD pattern is shown in Figure 3.1(b)) was transformed to an amorphous Li-Si alloy represented by the long plateau around 0.1 V [135].

Large amounts of SEI formation in this period resulted in relatively low 1^{st} cycle Coulombic efficiencies, which were 74%, 77%, 65% and 76% for PVDF, sodium alginate, Nafion and Li-Nafion containing electrodes, respectively. The charge capacities of all silicon electrodes, calculated based on silicon mass, became stable at 1200 mAh g^{-1} for more than 75 cycles. Then the charge capacity of the Si/PVDF system started to decrease which was followed by the Si/Nafion system. Surprisingly, the behavior of the Si/Nafion electrode in the full cell was different from the result in our previous report using half cells, in which both Nafion and Li-Nafion exhibited similar cycling

behavior [135]. The stable cycling behavior shown in Figure 4.1(a) is partially due to the relative small volumetric strain of silicon particles as they are partially lithiated when the charge capacity is limited to 1200 mAh g^{-1}. Figure 4.1(a) also demonstrates a significant improvement of the cycling performance of silicon electrodes in full cells by using Li-Nafion or sodium alginate binders compared with those using other binders, such as CMC [126][137].

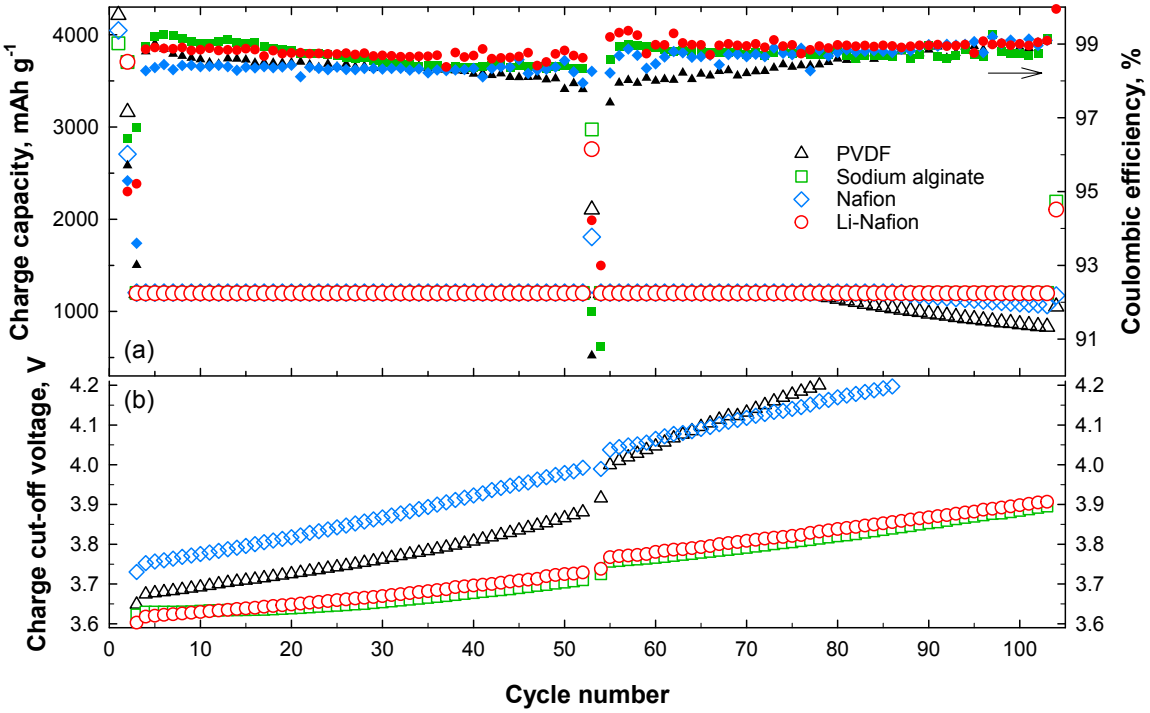

Figure 4.1: Electrochemical characteristics of silicon nanoparticles mixed with various binders under partial charge/discharge with a specific capacity limit of 1200 mAh g^{-1} in a voltage range from 4.2 V to 2.8 V: (a) Charge capacity and Coulombic efficiency (denoted by filled markers) vs. cycle number curves. For the 1^{st}, 2^{nd}, 53^{rd} and 104^{th} cycles, the C-rate was C/10, and there were no capacity limits; for all the other cycles, the C-rate was C/1. (b) Charge cut-off voltage vs. cycle number curves, for C/1 only.

Figure 4.1(b) shows the charge cut-off voltage evolution curves upon cycling at C/1. During cycling, the degradation of silicon electrodes can happen even though the capacity is limited to 1200 mAh g^{-1}. Because some silicon particles are isolated upon cycling, the remaining particles would take on more lithium and experience

greater volume expansion. The change of Li to Si ratio would cause the charge cut-off voltage to increase until the upper limit of 4.2 V is reached when the cell capacity starts to drop below 1200 mAh g^{-1}. Systems containing PVDF and Nafion reached the cut-off voltage of 4.2 V (the upper limit) when their charge capacities started to drop, while the ending voltages for systems containing sodium alginate and Li-Nafion were both around 3.9 V. Additionally, the slope of curves of the Si/sodium alginate and Si/Li-Nafion electrodes were very close to each other and were smaller than that for the Si/PVDF or Si/Nafion electrodes. This suggests longer cycle life would be achieved when sodium alginate or Li-Nafion are used.

After every 50 cycles, the coin cells were cycled at C/10 for 1 cycle without the capacity limitation. From Figure 4.1(a), after 50 cycles, the charge capacities were 2974 mAh g^{-1}, 2758 mAh g^{-1}, 1808 mAh g^{-1}, and 2105 mAh g^{-1} for electrodes containing sodium alginate, Li-Nafion, Nafion and PVDF, respectively. Furthermore, after 100 cycles, silicon mixed with sodium alginate or Li-Nafion electrodes could still maintain capacities more than 2100 mAh g^{-1}. In Figure 4.1(b), there is an apparent increase of the slope in the Si/PVDF electrode after 50 cycles which indicates the adverse influence of C/10 cycling associated with large volume changes.

4.4 Cycling Performance for the Full Charge/Discharge Test

To further explore the role of binders when silicon is suffering from more severe volume changes, new batches of electrodes were cycled at C/3 for 50 cycles preceded by two stabilization cycles at C/10 in a voltage window between 4.2 V and 2.8 V. This is called full charge/discharge cycling in this chapter. Discharge capacity curves and Coulombic efficiency curves are illustrated in Figure 4.2. Overall, all four types of electrodes experienced fast capacity fading in the initial 15 cycles with Coulombic efficiencies below 98% followed by slower capacity degradation. The capacity retention percentages after 50 cycles were 36%, 49%, 51% and 53% for electrodes containing

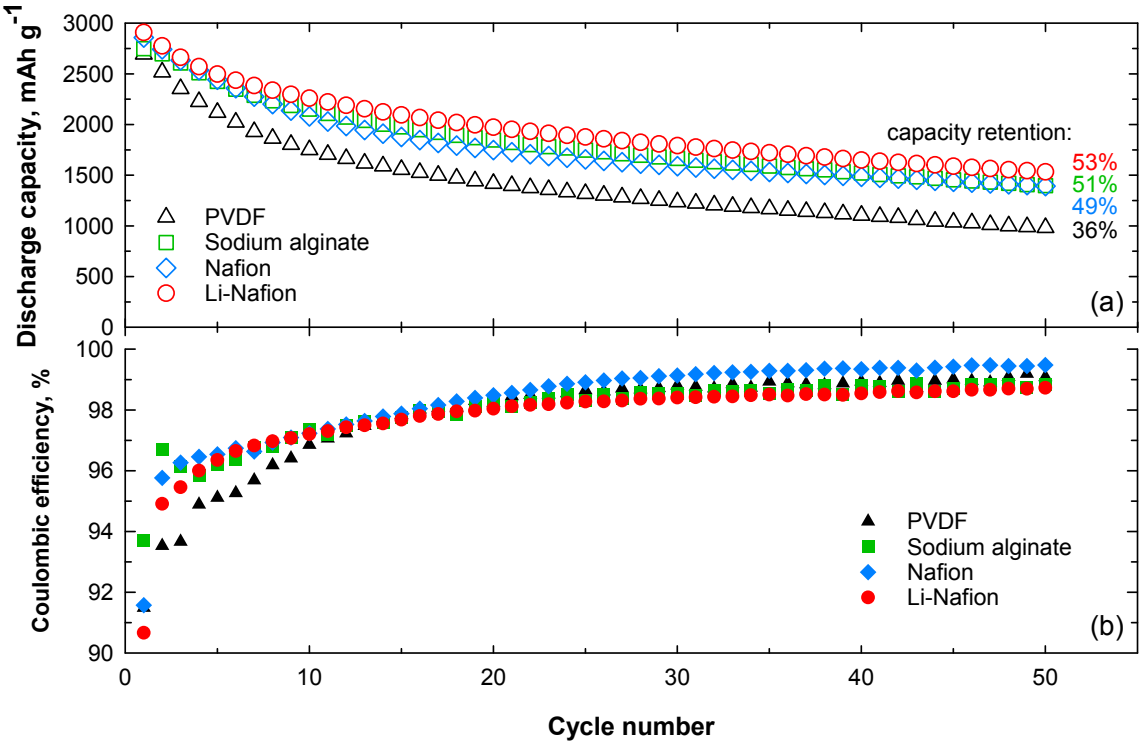

Figure 4.2: Electrochemical characteristics of silicon nanoparticles mixed with four different binders under full charge/discharge, the C-rate was C/3 and the voltage window was 4.2-2.8 V: (a) Discharge capacity vs. cycle number curves. (b) Coulombic efficiency vs. cycle number curves.

PVDF, Nafion, sodium alginate and Li-Nafion, respectively. In half cells with unlimited supply of lithium, silicon mixed with Nafion and sodium alginate binders were reported with high capacities and stable cycling for up to 100 cycles [110][135]. The failure mechanism of nano-sized silicon is generally summarized as the thickening of SEI layer on silicon particle surface or inside pores between particles [127][138]. Since we observed quite different behavior between our half cells and full cells, the failure mechanisms are not the same.

To better understand the behavior of full cells, voltages profiles during full charge or discharge cycling for the 1^{st}, 25^{th}, and 50^{th} cycles are plotted in Figure 4.3. For full cells, slippages of the charge and discharge capacity endpoints to the right upon cycling are attributed to parasitic reactions happening at both the positive electrode

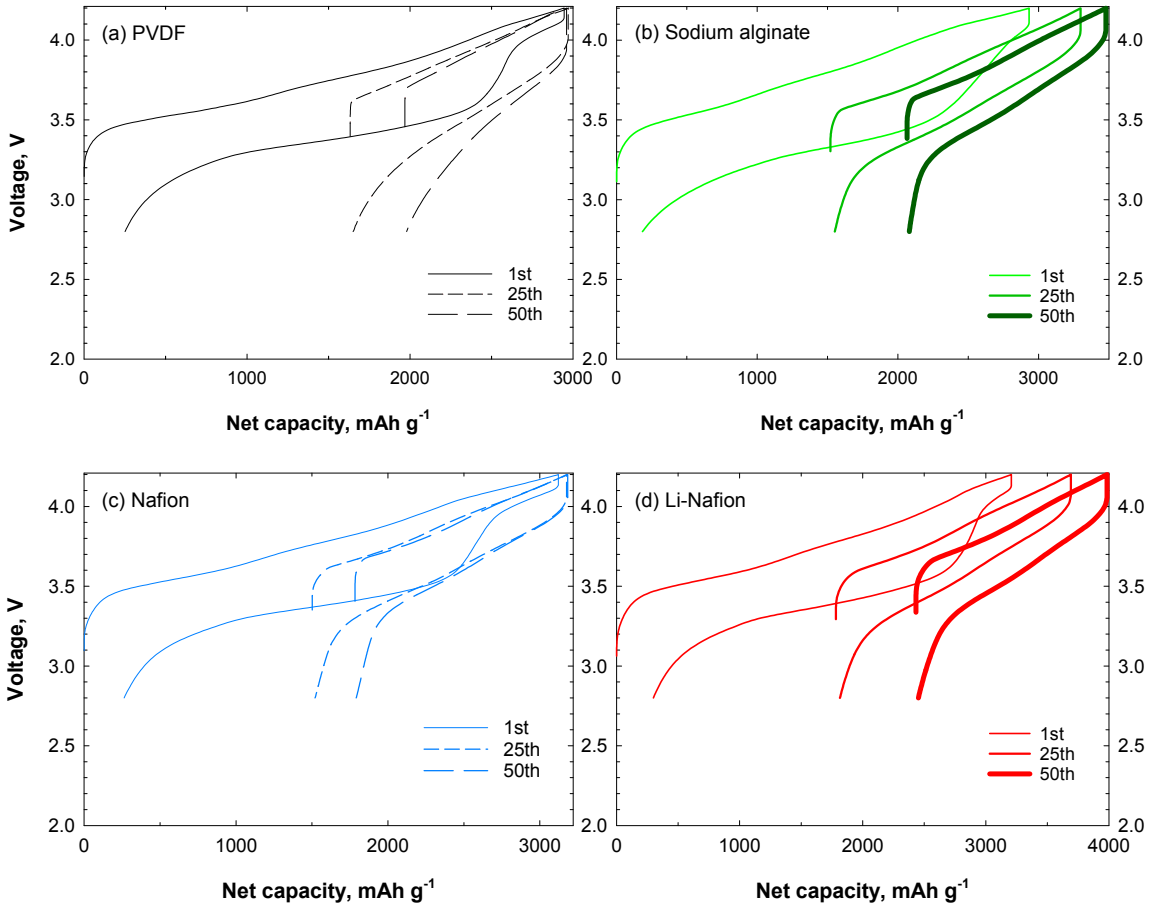

Figure 4.3: Voltage profiles of silicon electrodes mixed with different binders under full charge/discharge, the C-rate was C/3 and the voltage window was 4.2-2.8 V, including (a) PVDF, (b) Sodium alginate, (c) Nafion, and (d) Li-Nafion.

and negative electrode [97][98]. An explanation of the slippage mechanism has been discussed in Section 2.2. From Figure 4.3, slippages of the charge and discharge capacity endpoints for silicon mixed with Li-Nafion and sodium alginate are apparently much faster than that for silicon mixed with PVDF and Nafion. Indicated by the slopes calculated from the data after the initial 20 cycles, the net capacity or cumulative capacity (in mAh g^{-1}) curve shown in Figure 4.4 confirmed this observation.

Although the fast slippage of the charge and discharge capacity endpoints suggests more liquid electrolyte side reactions occurring at both the Si and NMC electrodes, it is unclear what reactions are happening. Nevertheless, these reactions do not seem

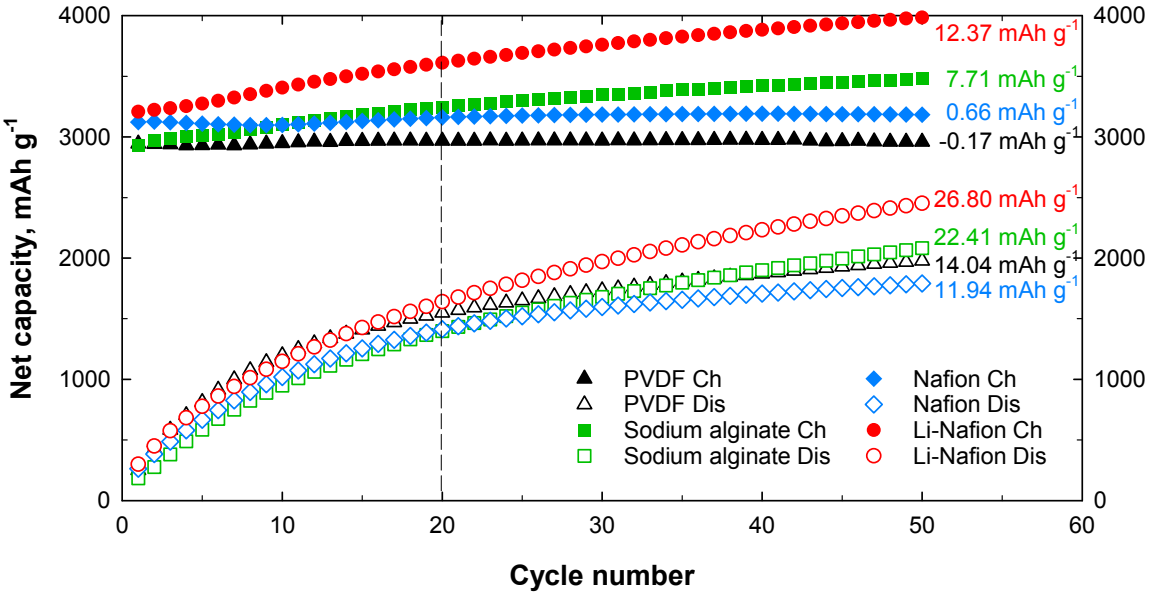

Figure 4.4: Net capacities of silicon electrodes mixed with different binders under full charge/discharge, the C-rate was C/3 and the voltage window was 4.2-2.8 V. Slopes of curves are calculated for the last 30 cycles only.

to facilitate capacity fading. As the Coulombic efficiency decreases with increasing rate of slippage of the discharge capacity endpoints [97], we observe that there is a good agreement between Figure 4.2(b) and 4.4.

In addition, the capacity fade rate is determined mathematically by the difference between slippage rates of the charge and discharge capacity endpoints [97]. Based on this knowledge, after the initial 20 cycles, the capacity fade rates for Si/Li-Nafion, Si/sodium alginate and Si/PVDF electrodes are around 14 mAh g^{-1} per cycle. While for the Si/Nafion electrode, the capacity fade rate is 11 mAh g^{-1} per cycle. On the other hand, from Figures 4.2(a) and 4.4, the capacity fade rates are apparently different in the initial 20 cycles. These results suggest that the role of binders in the early stage of cycling is decisive for the overall electrochemical performance of electrodes during full charge/discharge cycling.

Based on our analysis, for either half cells or full cells, both loss of active silicon particles and lithium consumption by parasitic reactions are contributing to the ca-

pacity fade. For full cells, more parasitic reactions consuming cycleable lithium are likely to result in faster failure of the cells. Therefore, the cycle life of full cells is much shorter than that of half cells. In either half cells or full cells, the cycling behavior of silicon electrodes can be greatly improved when Li-Nafion or sodium alginate binders are used.

4.5 Electrode Surface Morphology

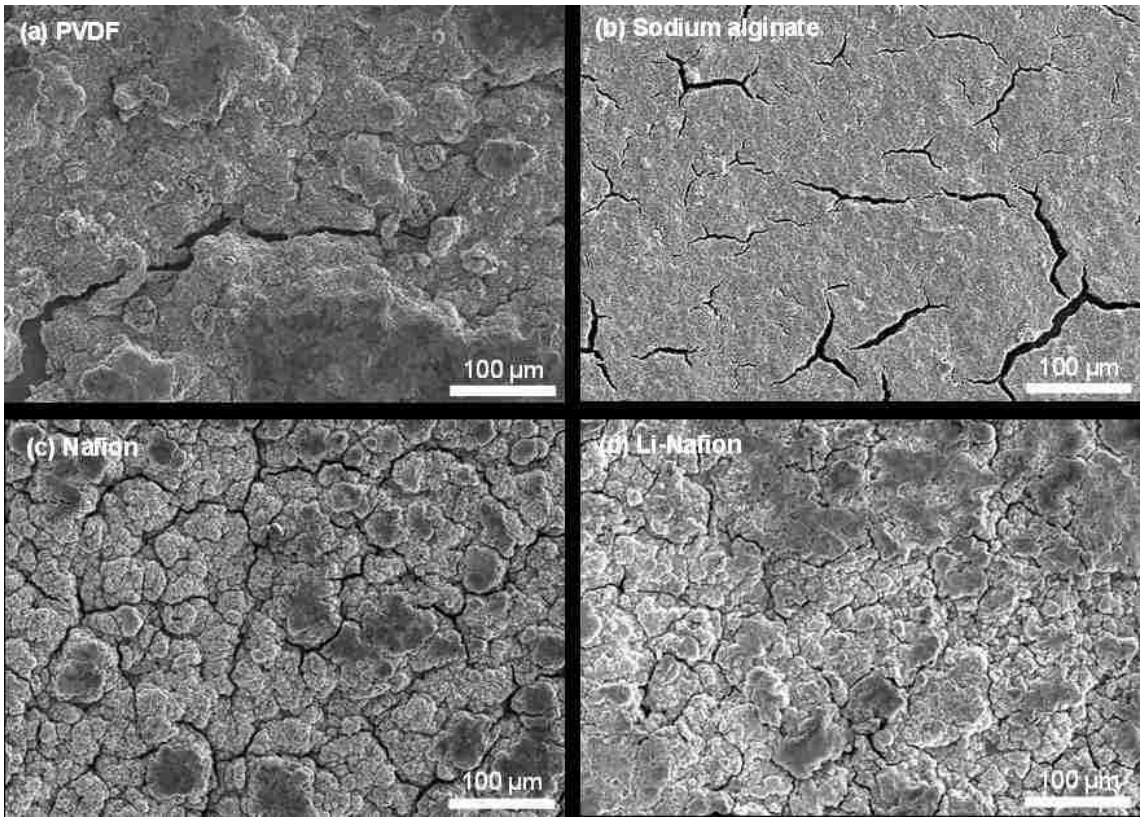

Figure 4.5: SEM images of silicon electrodes mixed with (a) PVDF, (b) Sodium alginate, (c) Nafion, and (d) Li-Nafion after 100 cycles at C/1 with a specific capacity limit of 1200 mAh g^{-1} in a voltage range from 4.2 V to 2.8 V.

Coin cells after partial charge/discharge cycling were opened to examine the surface morphology by SEM and the images of silicon electrodes are shown in Figure 4.5. Large and small cracks in all four types of electrodes were caused by continuous

expansion and contraction of silicon particles upon cycling. From Figure 3.1(a), the diameters of silicon nanoparticles we used range from 30 to 50 nm. Therefore, it is likely that disintegration of electrode, instead of cracking of silicon nanoparticle, is the main cause of degradation [139][140]. From Figure 4.5, we believe that the electrically isolated silicon nanoparticles after three-dimensional structure damage of electrodes are contributing directly to the capacity decrease and eventual failure of cells. Since no apparent delamination of electrodes from current collector was observed, we believe PVDF, sodium alginate, and Nafion binders all have sufficient binding capability to the copper substrate. However, their adhesion to silicon particles could be different. This difference is likely a key to the understanding of the effectiveness of binders on the performance of silicon electrodes.

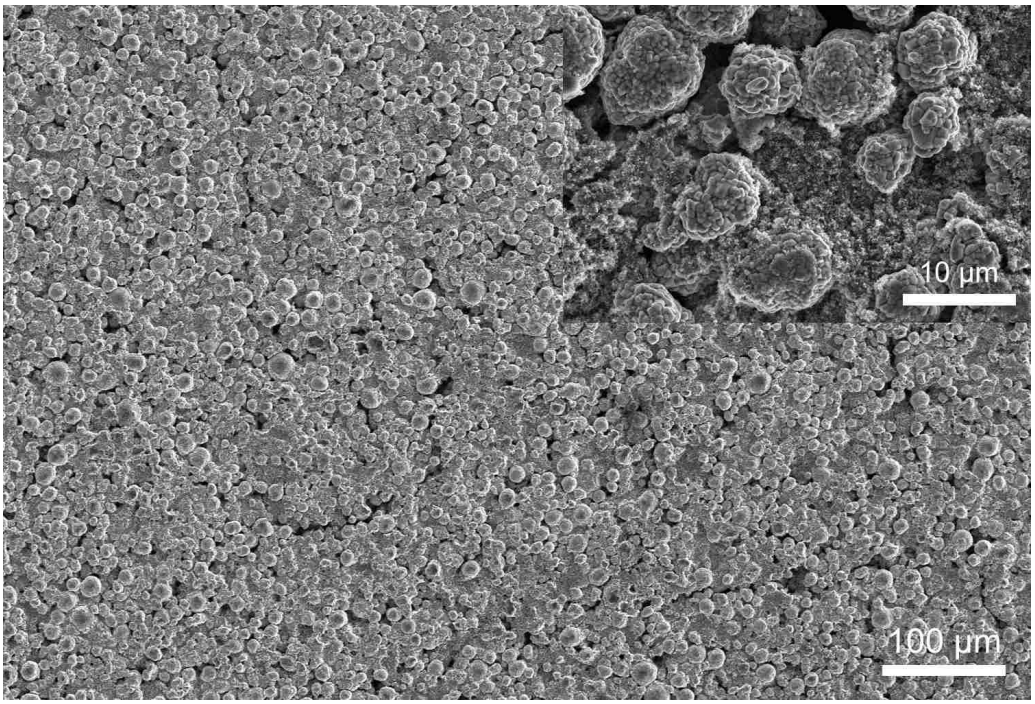

Figure 4.6: SEM image of the NMC electrode in the Si/Nafion full cell after 100 cycles at C/1 with a specific capacity limit of 1200 mAh g^{-1} in a voltage range from 4.2 V to 2.8 V.

On the other hand, as expected, all NMC electrodes were intact after 100 cycles. Because the NMC is a commercially mature positive electrode, we believe that the

structural integrity of NMC in our full cells is maintained. Take the Si/Nafion full cell as an example, the SEM image of its NMC electrode is shown in Figure 4.6.

4.6 XPS Spectra Analysis

XPS measurements were carried out to study the chemical composition of silicon electrode surface after the partial and full charge/discharge cycling tests for 100 and 50 cycles, respectively. Since the results are very similar for both tests, only the spectra for the partial charge/discharge testing are discussed. Normalized XPS spectra (C 1s, F 1s and Si 2p) for silicon electrodes containing different binders after 100 cycles between 4.2 V and 2.8 V at C/1 are presented in Figure 4.7. XPS measurements were conducted at two different spots on each electrode, only one set of data is presented here.

In Figure 4.7(a), the C-C peak located around 285 eV, which is usually associated with the carbon black and alkane species or surface hydrocarbon contamination, is invisible for all the binders. The intensity of the C-C peak could be very low and it is overwhelmed by the broad peak ranging from 284 eV to 288 eV. This phenomenon was once observed by another group, while it is still different from some reports in which there are strong C-C peaks [110][118][122]. The peak around 286 eV is assigned to the C-O bonds in carbonaceous solvent reduction products (e.g., ethers ROLi and esters RCOOLi) and the peak at 288.5 eV can be attributed to the O-C=O bond in alkyl carbonate solutions [122][123]. The weak peak around 291 eV in the Si/Li-Nafion system indicates less lithium carbonates and less lithium alkyl carbonate solutions formed on silicon surfaces.

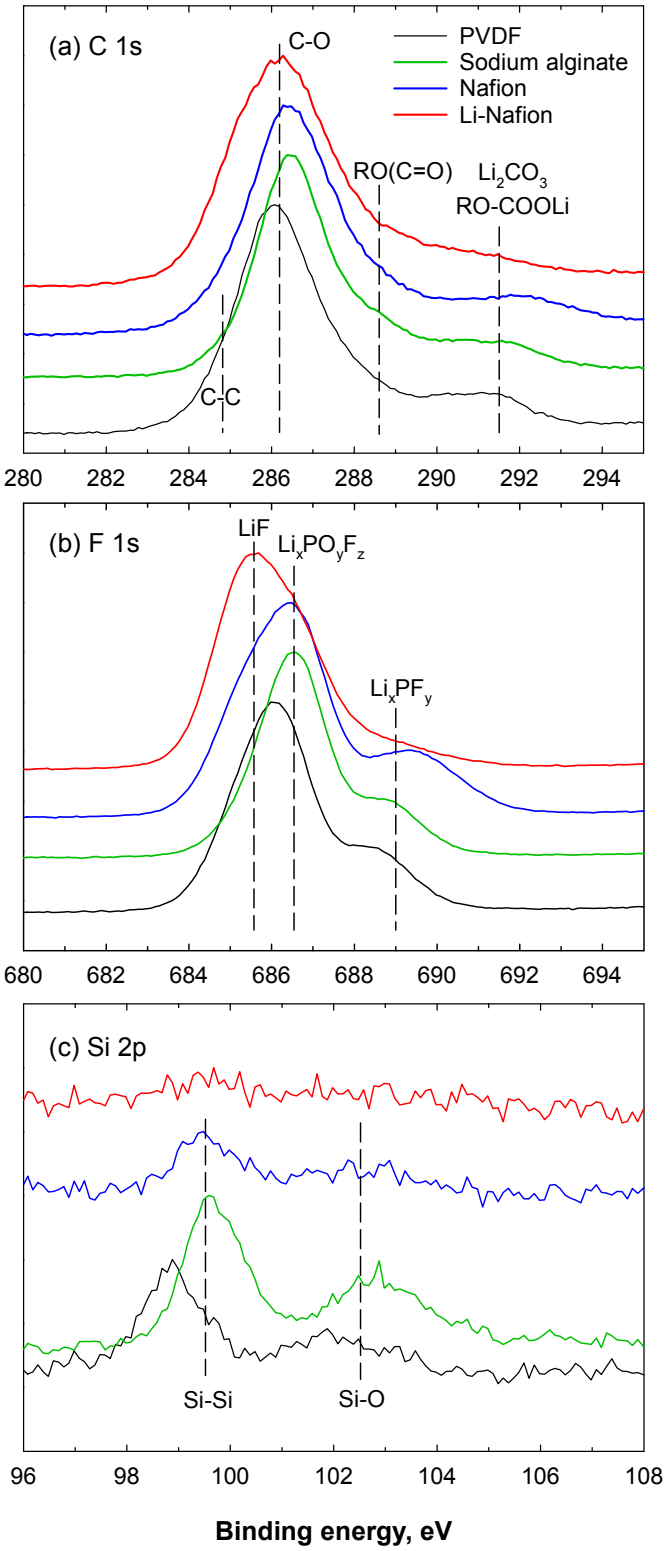

Figure 4.7: XPS spectra of silicon nanoparticles mixed with various binders under partial charge/discharge after 100 cycles at C/1 with a specific capacity limit of 1200 mAh g^{-1} in a voltage range from 4.2 V to 2.8 V: (a) C 1s peaks. (b) F 1s peaks. (c) Si 2p peaks.

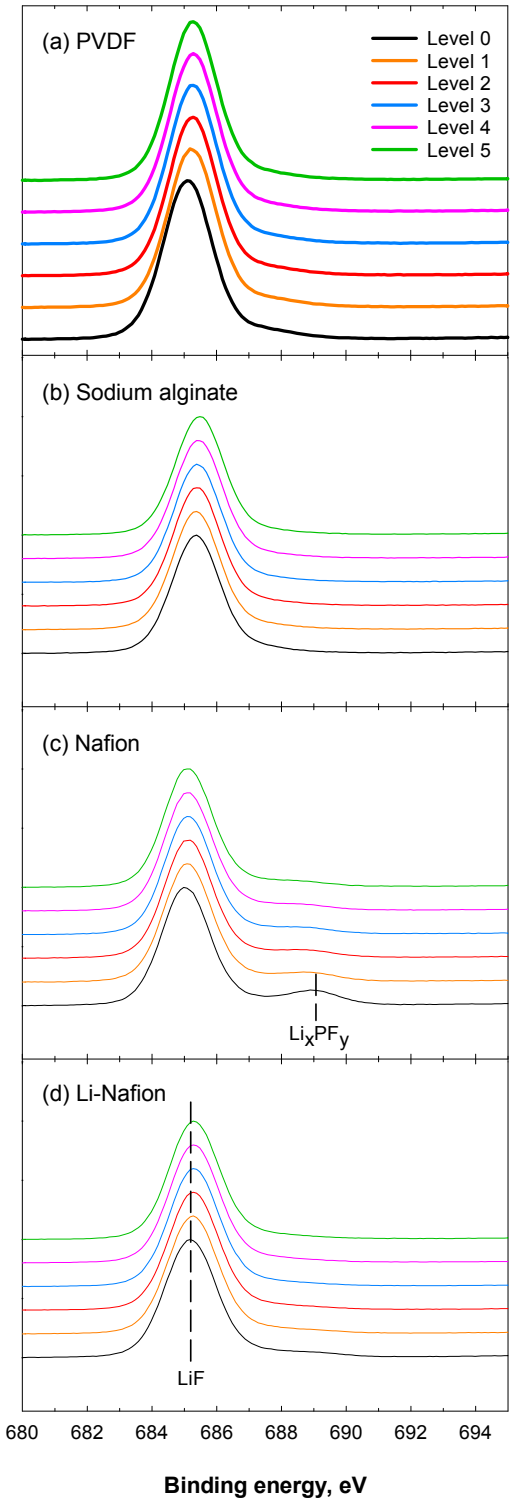

Figure 4.8: XPS F 1s peaks during depth profile measurements of silicon nanoparticles mixed with various binders under partial charge/discharge after 100 cycles at C/1 with a specific capacity limit of 1200 mAh g^{-1} in the voltage range from 4.2 V to 2.8 V: (a) PVDF, (b) sodium alginate, (c) Nafion and (d) Li-Nafion. Ion gun energy is 2 keV, and each etch step lasts for 4 s using the medium current.

From Figure 4.7(b), the broad peak ranging from 684 eV to 688 eV is composed of the LiF peak around 685.5 eV and the $Li_xPO_yF_z$ peak around 686.5 eV [118]. The peak at around 689 eV indicates the presence of another electrolyte salt product Li_xPF_y. As shown in Figure 4.8, the depth profiles show that the Li_xPF_y peaks disappear after the silicon surfaces were etched for 4 seconds. This indicates the electrolyte salt is likely to decompose only to LiF, which forms one of the key inorganic components of SEI layer. As illustrated in Figure 4.7(c), strong Si-Si peaks around 99 eV detected in Si/PVDF, Si/sodium alginate and Si/Nafion electrodes were understood as the exposure of silicon surfaces compared with the results after 10 cycles in half cells [135]. While for the Si/Li-Nafion electrode, the weak Si-Si signal is possibly due to the SEI layer covered on silicon particles, which is beneficial for the performance. The Si-O peaks around 103 eV found in the Si/sodium alginate and Si/PVDF electrodes most probably suggest the presence of SiO_x and Li_xSiO_y phases, which are likely to form by silicon-electrolyte reactions [122][126]. Since no apparent difference in the SEI layer composition was observed on silicon electrodes containing various binders in our study, we believe that the failure of any full cell is mainly due to the loss of active silicon and the thickening of the SEI layer on the silicon electrode.

In the introduction section, we mention there are several essential characteristics of binders proposed to ensure good battery performance. One of them is the mechanical properties of binders. The mechanical properties of several commonly studied binders for silicon electrodes have been measured using tensile tests and atomic force microscopy indentation tests to explain binding mechanisms [60][104][110][141]. When immersed in the organic electrolyte, it was reported that PVDF became much softer and thus it was only suitable for electrodes that would not experience huge volume changes upon charge/discharge [104][110]. However, it is quite possible that the mechanical properties of bulk polymer are different from that in the form of binders in porous electrodes. For thin polymer films, using nanoindentation technique under

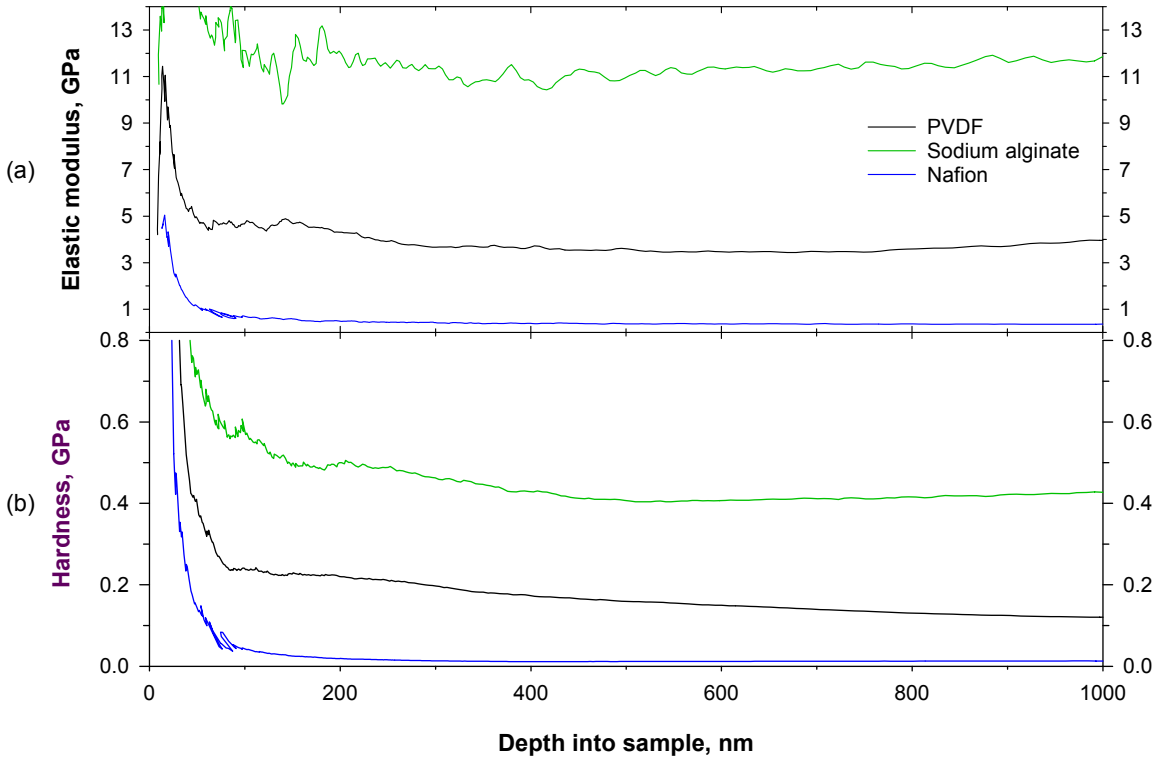

Figure 4.9: Elastic modulus (a) and hardness (b) of dry polymer films measured by nanoindentation using the continuous stiffness measurement mode.

continuous stiffness measurement mode, we are able to obtain their elastic modulus and hardness values as shown in Figure 4.9. The results show that sodium alginate exhibits very high elastic modulus and hardness and it is therefore a robust binder. In contrast, the effective Nafion binder has very low elastic modulus and hardness. Since both robust sodium alginate and soft Nafion are very good binders with drastically different mechanical properties, we conclude that the mechanical properties of binder materials alone are insufficient to predict their efficacies as binders in the composite electrodes consisting silicon nanoparticles, carbon black, and binders. Furthermore, compared with the simple molecular chain of PVDF, it is generally believed that the hydrogen bonding between carboxylic acid groups in sodium alginate is contributing to the good adhesion between binder and silicon particles, leading to good cycling behavior. For Nafion binders, there are no available hydrogen bonds. Their capabili-

ties to transport Li^+ to silicon particles and effective binding capability could be used to explain the promising cycling performance in both full cells and half cells [135]. The adhesion between PVDF and silicon particles is likely to be inferior to that between Nafion or sodium alginate and silicon particles based on the electrochemical performance.

Overall, the failure mechanisms of silicon nanoparticles are described in a schematic diagram in Figure 4.10. Coupled chemical degradation (SEI growth, lithium consumption) and mechanical degradation (cracking, particles isolation) are the cause of the failure of the full cells.

4.7 Summary

Si/NMC full cells were tested to better understand the role of polymeric binders, including PVDF, sodium alginate, Nafion and Li-Nafion. From the partial charge/discharge test, we learn that silicon nanoparticles mixed with Li-Nafion or sodium alginate as binders can achieve stable capacity of 1200 mAh g^{-1} for more than 100 cycles. From the full charge/discharge test involving even larger volume changes, we observe higher capacity retention percentages for silicon nanoparticles mixed with sodium alginate or Nafion binders compared with that using the traditional PVDF binder.

XPS measurement further indicates that binders will not change the composition of SEI formed at the silicon electrodes. Therefore, silicon loss and SEI growth are the main causes for the failure of the full cells. In addition, combined with elastic modulus and hardness measurement using nanoindentation technique, we conclude that the mechanical properties of binder alone cannot predict the effectiveness of the binders in composite silicon electrodes that experience the large volume changes. This work not only studies the performance of well-established binders for silicon nanoparticles in lithium-ion full cells systematically but also inspires new directions to overcome existing challenges of silicon electrode, for instance, developing novel electrolyte ad-

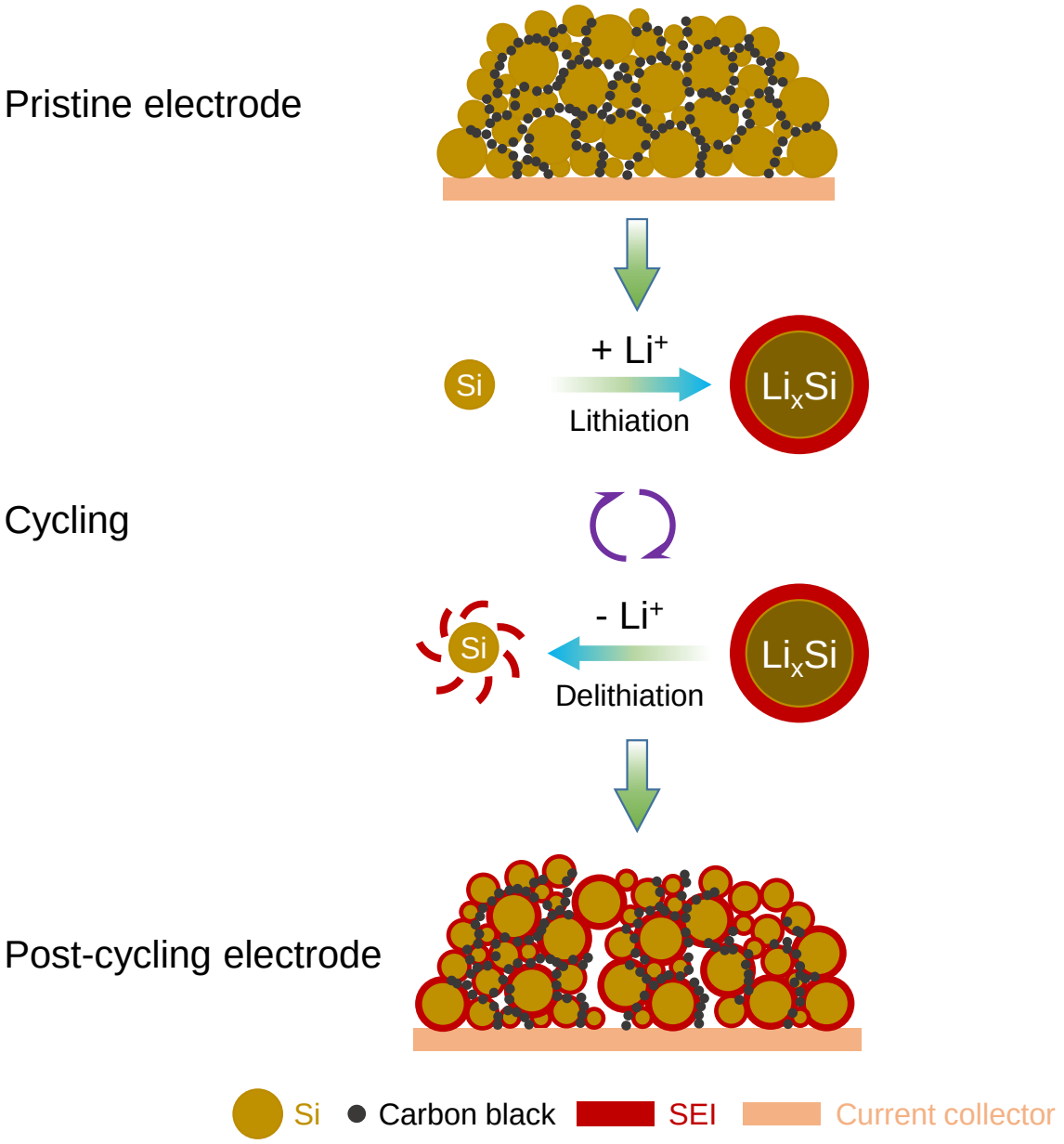

Figure 4.10: A schematic plot of the failure mechanisms of silicon nanoparticles.

ditives to stabilize the SEI layer and polymeric coatings on silicon particles or binders to enhance the electrode integrity.

Chapter 5 Conclusions and Future Work

5.1 Conclusions

Through our effort of integrating various approaches, including cycleable silicon nanoparticles, polymeric binders and electrolyte additive, several important aspects towards advancing the silicon negative electrodes for applications in the next generation LIBs are confirmed and understood as:

(1) *Effective polymeric binders.* As a porous electrode is made of active silicon, polymer binder and conductive additive, the choice of binder is critical for the performance of silicon electrodes experiencing large volumetric strain upon cycling. Nafion, ion-exchange Nafion and sodium alginate are demonstrated as effective binders of silicon electrodes by accomplishing high capacity (> 1200 mAh g^{-1}) and relatively long cycle life (> 100 cycles) compared with the traditional binder PVDF in both half cells and full cells (Si/NMC). It is further inferred that the behavior of binder in the early stage of cycling is decisive for the overall performance of silicon electrodes.

(2) *Partial charge/discharge vs. full charge/discharge.* Partial charge/discharge with controlled capacity limits the mechanical strain induced to the electrodes and therefore prolongs the cycle life significantly, especially when ion-exchanged Nafion and sodium alginate are used as binders. In realistic operations, partial charge or discharge can be achieved by regulating voltages.

(3) *SEI composition and side reactions.* During cycling, the thin SEI layer formed on the silicon surface is assumed to experience expansion and contraction as well. The fracture of SEI layer will expose fresh silicon surface to the electrolyte, causing formation of new SEI. This continuous mechanism, generally named chemical degradation, is mainly responsible for the lithium loss in a cell. The side reactions are happening on both the negative and positive electrodes in the full cells. Based on the

experimental results, more side reactions happened in Si/Li-Nafion and Si/sodium alginates electrodes would not facilitate the capacity fading. This phenomenon implies the interactions of side reactions between the negative electrode and positive electrode. In addition, XPS measurements show that there is no apparent difference between SEI compositions when four types of binders are present.

(4) *Interactions between binders and silicon particles.* Though it is frequently hypothesized that the interactions (e.g. bonding) between binders and silicon are beneficial for the performance, these mechanisms in a complex battery system are not easy to verify. In fact, binders are expected to be stable in the electrolyte. At least, they are not supposed to participate in chemical reactions, for example, the SEI compositions in different electrodes are similar as mentioned early. In this dissertation, ion-exchanged Nafion and sodium alginate are proved to slow the capacity fading with unclear mechanisms.

(5) *Failure mechanisms.* Coupled chemical degradation and mechanical degradation are contributing to the failure of the half cells and full cells. In half cells, lithium supply from the counter/reference electrode is unlimited, therefore the mechanical degradation is dominate over the chemical degradation to determine the capacity fading. However, in full cells, the lithium supply from the NMC is limited, thus the capacity fading rate is mainly determined by the consumption rate of lithium. This is the reason for the fast capacity decay in the full cells under full charge/discharge.

(6) *Role of mechanical properties of binders.* Binders are generally proposed to accommodate the large volume changes associated with Li-Si reactions. Our results unveil that both soft Nafion and robust sodium alginate are effective binders in half cells and full cells. Herein, we conclude that the mechanical properties of binders alone are not sufficient to predict the performance.

5.2 Future Work

Based on above conclusions and my understanding, several directions to further improve the electrochemical behavior of silicon electrodes are summarized as:

(1) *Novel electrolyte to stabilize the SEI.* The electrolyte additive is believed to decompose on the silicon surface prior to the electrolyte components themselves. Therefore the development of novel electrolyte and additives to stabilize the SEI is an effective way to reduce the chemical degradation and to slow the overall capacity fading when the magnitude of mechanical stress is under control.

(2) *Novel binders and polymeric coatings on silicon particles.* Because the disintegration of electrodes is unavoidable, if the isolated silicon particles are still connected in a conductive network maintained by novel binders or polymeric coatings, they will be involved in electrode reactions and the performance could be improved.

References

[1] D. Linden, T.B. Reddy, Handbook of Batteries, 3rd ed., McGraw-Hill, New York, 2002.

[2] R.J. Silbey, R.A. Alberty, Physical Chemistry, 3rd ed., Wiley, New York, 2001.

[3] W. Martienssen, H. Warlimont, Springer Handbook of Condensed Matter and Materials Data, Springer, Heidelberg ; New York, 2005.

[4] R.A. Huggins, Lithium Alloy Negative Electrodes, J Power Sources, 81 (1999) 13-19.

[5] W.J. Zhang, Lithium Insertion/Extraction Mechanism in Alloy Anodes for Lithium-Ion Batteries, J Power Sources, 196 (2011) 877-885.

[6] T. Ohzuku, Y. Iwakoshi, K. Sawai, Formation of Lithium-Graphite Intercalation Compounds in Nonaqueous Electrolytes and Their Application as a Negative Electrode for a Lithium Ion (Shuttlecock) Cell, J Electrochem Soc, 140 (1993) 2490-2498.

[7] J.R. Dahn, T. Zheng, Y.H. Liu, J.S. Xue, Mechanisms for Lithium Insertion in Carbonaceous Materials, Science, 270 (1995) 590-593.

[8] K. Sato, M. Noguchi, A. Demachi, N. Oki, M. Endo, A Mechanism of Lithium Storage in Disordered Carbons, Science, 264 (1994) 556-558.

[9] B.M. Way, J.R. Dahn, The Effect of Boron Substitution in Carbon on the Intercalation of Lithium in $Li_x(B_zC_{1-z})_6$, J Electrochem Soc, 141 (1994) 907-912.

[10] M. Inaba, H. Yoshida, Z. Ogumi, In Situ Raman Study of Electrochemical Lithium Insertion into Mesocarbon Microbeads Heat-Treated at Various Temperature, J Electrochem Soc, 143 (1996) 2572-2578.

[11] R. Alcantara, F.J.F. Madrigal, P. Lavela, J.L. Tirado, J.M.J. Mateos, C.G. de Salazar, R. Stoyanova, E. Zhecheva, Characterisation of Mesocarbon Microbeads (MCMB) as Active Electrode Material in Lithium and Sodium Cells, Carbon, 38 (2000) 1031-1041.

[12] B. Gao, C. Bower, J.D. Lorentzen, L. Fleming, A. Kleinhammes, X.P. Tang, L.E. McNeil, Y. Wu, O. Zhou, Enhanced Saturation Lithium Composition in Ball-Milled Single-Walled Carbon Nanotubes, Chem Phys Lett, 327 (2000) 69-75.

[13] C. de las Casas, W.Z. Li, A Review of Application of Carbon Nanotubes for Lithium Ion Battery Anode Material, J Power Sources, 208 (2012) 74-85.

[14] J.O. Besenhard, J. Yang, M. Winter, Will Advanced Lithium-Alloy Anodes Have a Chance in Lithium-Ion Batteries?, J Power Sources, 68 (1997) 87-90.

[15] M. Winter, J.O. Besenhard, Electrochemical Lithiation of Tin and Tin-Based Intermetallics and Composites, Electrochim Acta, 45 (1999) 31-50.

[16] B. Laforge, L. Levan-Jodin, R. Salot, A. Billard, Study of Germanium as Electrode in Thin-Film Battery, J Electrochem Soc, 155 (2008) A181-A188.

[17] L. Baggetto, P.H.L. Notten, Lithium-Ion (De)Insertion Reaction of Germanium Thin-Film Electrodes: An Electrochemical and In Situ XRD Study, J Electrochem Soc, 156 (2009) A169-A175.

[18] C.J. Wen, R.A. Huggins, Electrochemical Investigation of the Lithium-Gallium System, J Electrochem Soc, 128 (1981) 1636-1641.

[19] J. Saint, M. Morcrette, D. Larcher, J.M. Tarascon, Exploring the Li-Ga Room Temperature Phase Diagram and the Electrochemical Performances of the Li_xGa_y Alloys vs. Li, Solid State Ionics, 176 (2005) 189-197.

[20] K.T. Lee, Y.S. Jung, T. Kim, C.H. Kim, J.H. Kim, J.Y. Kwon, S.M. Oh, Liquid Gallium Electrode Confined in Porous Carbon Matrix as Anode for Lithium Secondary Batteries, Electrochem Solid St, 11 (2008) A21-A24.

[21] R.D. Deshpande, J.C. Li, Y.T. Cheng, M.W. Verbrugge, Liquid Metal Alloys as Self-Healing Negative Electrodes for Lithium Ion Batteries, J Electrochem Soc, 158 (2011) A845-A849.

[22] M. Wachtler, J.O. Besenhard, M. Winter, Tin and Tin-Based Intermetallics as New Anode Materials for Lithium-Ion Cells, J Power Sources, 94 (2001) 189-193.

[23] L.Y. Beaulieu, T.D. Hatchard, A. Bonakdarpour, M.D. Fleischauer, J.R. Dahn, Reaction of Li with Alloy Thin Films Studied by In Situ AFM, J Electrochem Soc, 150 (2003) A1457-A1464.

[24] Z.G. Yang, D. Choi, S. Kerisit, K.M. Rosso, D.H. Wang, J. Zhang, G. Graff, J. Liu, Nanostructures and Lithium Electrochemical Reactivity of Lithium Titanites and Titanium Oxides: A Review, J Power Sources, 192 (2009) 588-598.

[25] H.G. Jung, M.W. Jang, J. Hassoun, Y.K. Sun, B. Scrosati, A High-Rate Long-Life $Li_4Ti_5O_{12}/Li[Ni_{0.45}Co_{0.1}Mn_{1.45}]O_4$ Lithium-Ion Battery, Nat Commun, 2 (2011).

[26] E. Ferg, R.J. Gummow, A. Dekock, M.M. Thackeray, Spinel Anodes for Lithium-Ion Batteries, J Electrochem Soc, 141 (1994) L147-L150.

[27] S.L. Chou, J.Z. Wang, H.K. Liu, S.X. Dou, Rapid Synthesis of $Li_4Ti_5O_{12}$ Microspheres as Anode Materials and Its Binder Effect for Lithium-Ion Battery, J Phys Chem C, 115 (2011) 16220-16227.

[28] M.V. Reddy, G.V.S. Rao, B.V.R. Chowdari, Metal Oxides and Oxysalts as Anode Materials for Li Ion Batteries, Chem Rev, 113 (2013) 5364-5457.

[29] D. Larcher, S. Beattie, M. Morcrette, K. Edstroem, J.C. Jumas, J.M. Tarascon, Recent Findings and Prospects in the Field of Pure Metals as Negative Electrodes for Li-ion Batteries, J Mater Chem, 17 (2007) 3759-3772.

[30] U. Kasavajjula, C.S. Wang, A.J. Appleby, Nano- and Bulk-Silicon-Based Insertion Anodes for Lithium-Ion Secondary Cells, J Power Sources, 163 (2007) 1003-1039.

[31] M. Winter, J.O. Besenhard, M.E. Spahr, P. Novák, Insertion Electrode Materials for Rechargeable Lithium Batteries, Adv Mater, 10 (1998) 725-763.

[32] L.Y. Beaulieu, K.W. Eberman, R.L. Turner, L.J. Krause, J.R. Dahn, Colossal Reversible Volume Changes in Lithium Alloys, Electrochem Solid St, 4 (2001) A137-A140.

[33] V.G. Khomenko, V.Z. Barsukov, Characterization of Silicon- and Carbon-Based Composite Anodes for Lithium-Ion Batteries, Electrochim Acta, 52 (2007) 2829-2840.

[34] T. Takamura, S. Ohara, M. Uehara, J. Suzuki, K. Sekine, A Vacuum Deposited Si Film Having a Li Extraction Capacity over 2000 mAh/g with a Long Cycle Life, J Power Sources, 129 (2004) 96-100.

[35] T.L. Kulova, A.M. Skundin, Y.V. Pleskov, E.I. Terukov, O.I. Kon'kov, Lithium Insertion into Amorphous Silicon Thin-Film Electrodes, J Electroanal Chem, 600 (2007) 217-225.

[36] J. Graetz, C.C. Ahn, R. Yazami, B. Fultz, Highly Reversible Lithium Storage in Nanostructured Silicon, Electrochem Solid St, 6 (2003) A194-A197.

[37] C.K. Chan, H.L. Peng, G. Liu, K. McIlwrath, X.F. Zhang, R.A. Huggins, Y. Cui, High-Performance Lithium Battery Anodes Using Silicon Nanowires, Nat Nanotechnol, 3 (2008) 31-35.

[38] X. Xiao, P. Liu, M.W. Verbrugge, H. Haftbaradaran, H. Gao, Improved Cycling Stability of Silicon Thin Film Electrodes through Patterning for High Energy Density Lithium Batteries, J Power Sources, 196 (2011) 1409-1416.

[39] H. Wu, G. Chan, J.W. Choi, I. Ryu, Y. Yao, M.T. McDowell, S.W. Lee, A. Jackson, Y. Yang, L.B. Hu, Y. Cui, Stable Cycling of Double-Walled Silicon Nanotube Battery Anodes through Solid-Electrolyte Interphase Control, Nat Nanotechnol, 7 (2012) 309-314.

[40] G.X. Wang, J.H. Ahn, M.J. Lindsay, L. Sun, D.H. Bradhurst, S.X. Dou, H.K. Liu, Graphite-Tin Composites as Anode Materials for Lithium-Ion Batteries, J Power Sources, 97-8 (2001) 211-215.

[41] M.K. Datta, P.N. Kumta, Silicon and Carbon Based Composite Anodes for Lithium Ion Batteries, J Power Sources, 158 (2006) 557-563.

[42] M. Holzapfel, H. Buqa, W. Scheifele, P. Novák, F.M. Petrat, A New Type of Nano-Sized Silicon/Carbon Composite Electrode for Reversible Lithium Insertion, Chem Commun, (2005) 1566-1568.

[43] L.F. Cui, Y. Yang, C.M. Hsu, Y. Cui, Carbon-Silicon Core-Shell Nanowires as High Capacity Electrode for Lithium Ion Batteries, Nano Lett, 9 (2009) 3370-3374.

[44] J.O. Besenhard, Handbook of Battery Materials, Wiley-VCH, Weinheim ; New York, 1999.

[45] G.G. Amatucci, J.M. Tarascon, L.C. Klein, Cobalt Dissolution in $LiCoO_2$-Based Non-Aqueous Rechargeable Batteries, Solid State Ionics, 83 (1996) 167-173.

[46] S. Venkatraman, Y. Shin, A. Manthiram, Phase Relationships and Structural and Chemical Stabilities of Charged $Li_{1-x}CoO_{2-\delta}$ and $Li_{1-x}Ni_{0.85}Co_{0.15}O_{2-\delta}$ Cathodes, Electrochem Solid St, 6 (2003) A9-A12.

[47] Z.H. Lu, D.D. MacNeil, J.R. Dahn, Layered Cathode Materials $Li[Ni_xLi_{(1/3-2x/3)}$-$Mn_{(2/3-x/3)}]O_2$ for Lithium-Ion Batteries, Electrochem Solid St, 4 (2001) A191-A194.

[48] N. Yabuuchi, T. Ohzuku, Novel Lithium Insertion Material of $LiCo_{1/3}Ni_{1/3}Mn_{1/3}$-$O_2$ for Advanced Lithium-Ion Batteries, J Power Sources, 119 (2003) 171-174.

[49] D.C. Li, C.Q. Yuan, J.Q. Dong, Z.H. Peng, Y.H. Zhou, Synthesis and Electrochemical Properties of $LiNi_{0.85-x}Co_xMn_{0.15}O_2$ as Cathode Materials for Lithium-Ion Batteries, J Solid State Electr, 12 (2008) 323-327.

[50] C.H. Lu, Y.K. Lin, Microemulsion Preparation and Electrochemical Characteristics of $LiNi_{1/3}Co_{1/3}Mn_{1/3}O_2$ Powders, J Power Sources, 189 (2009) 40-44.

[51] S.K. Martha, H. Sclar, Z.S. Framowitz, D. Kovacheva, N. Saliyski, Y. Gofer, P. Sharon, E. Golik, B. Markovsky, D. Aurbach, A Comparative Study of Electrodes Comprising Nanometric and Submicron Particles of $LiNi_{0.50}Mn_{0.50}O_2$, $LiNi_{0.33}$-$Mn_{0.33}Co_{0.33}O_2$, and $LiNi_{0.40}Mn_{0.40}Co_{0.20}O_2$ Layered Compounds, J Power Sources, 189 (2009) 248-255.

[52] J.W. Fergus, Recent Developments in Cathode Materials for Lithium Ion Batteries, J Power Sources, 195 (2010) 939-954.

[53] M. Yoshio, R.J. Brodd, A. Kozawa, Lithium-Ion Batteries Science and Technologies, Springer-Verlag New York, New York, 2009.

[54] B. Xu, D.N. Qian, Z.Y. Wang, Y.S.L. Meng, Recent Progress in Cathode Materials Research for Advanced Lithium Ion Batteries, Mat Sci Eng R, 73 (2012) 51-65.

[55] M. Armand, The History of Polymer Electrolytes, Solid State Ionics, 69 (1994) 309-319.

[56] J.M. Tarascon, A.S. Gozdz, C. Schmutz, F. Shokoohi, P.C. Warren, Performance of Bellcore's Plastic Rechargeable Li-Ion Batteries, Solid State Ionics, 86-8 (1996) 49-54.

[57] N.S. Choi, Y.G. Lee, J.K. Park, Effect of Cathode Binder on Electrochemical Properties of Lithium Rechargeable Polymer Batteries, J Power Sources, 112 (2002) 61-66.

[58] Z.H. Chen, L. Christensen, J.R. Dahn, Large-Volume-Change Electrodes for Li-ion Batteries of Amorphous Alloy Particles Held by Elastomeric Tethers, Electrochem Commun, 5 (2003) 919-923.

[59] J. Li, R.B. Lewis, J.R. Dahn, Sodium carboxymethyl cellulose - A Potential Binder for Si Negative Electrodes for Li-Ion Batteries, Electrochem Solid St, 10 (2007) A17-A20.

[60] R.R. Garsuch, D.B. Le, A. Garsuch, J. Li, S. Wang, A. Farooq, J.R. Dahn, Studies of Lithium-Exchanged Nafion as an Electrode Binder for Alloy Negatives in Lithium-Ion Batteries, J Electrochem Soc, 155 (2008) A721-A724.

[61] G. Liu, S.D. Xun, N. Vukmirovic, X.Y. Song, P. Olalde-Velasco, H.H. Zheng, V.S. Battaglia, L.W. Wang, W.L. Yang, Polymers with Tailored Electronic Structure for High Capacity Lithium Battery Electrodes, Adv Mater, 23 (2011) 4679.

[62] M.Y. Wu, X.C. Xiao, N. Vukmirovic, S.D. Xun, P.K. Das, X.Y. Song, P. Olalde-Velasco, D.D. Wang, A.Z. Weber, L.W. Wang, V.S. Battaglia, W.L. Yang, G. Liu, Toward an Ideal Polymer Binder Design for High-Capacity Battery Anodes, J Am Chem Soc, 135 (2013) 12048-12056.

[63] http://www.uscar.org/guest/publications.php

[64] J. Vetter, P. Novák, M.R. Wagner, C. Veit, K.C. Möller, J.O. Besenhard, M. Winter, M. Wohlfahrt-Mehrens, C. Vogler, A. Hammouche, Ageing Mechanisms in Lithium-Ion Batteries, J Power Sources, 147 (2005) 269-281.

[65] R.J. Gummow, A. Dekock, M.M. Thackeray, Improved Capacity Retention in Rechargeable 4 V Lithium/Lithium Manganese Oxide (Spinel) Cells, Solid State Ionics, 69 (1994) 59-67.

[66] M.M. Thackeray, Y. Shao-Horn, A.J. Kahaian, K.D. Kepler, J.T. Vaughey, S.A. Hackney, Structural Fatigue in Spinel Electrodes in High Voltage (4V) Li/Li_xMn_2-O_4 Cells, Electrochem Solid St, 1 (1998) 7-9.

[67] M. Broussely, S. Herreyre, P. Biensan, P. Kasztejna, K. Nechev, R.J. Staniewicz, Aging Mechanism in Li Ion Cells and Calendar Life Predictions, J Power Sources, 97-8 (2001) 13-21.

[68] P. Liu, J. Wang, J. Hicks-Garner, E. Sherman, S. Soukiazian, M. Verbrugge, H. Tataria, J. Musser, P. Finamore, Aging Mechanisms of $LiFePO_4$ Batteries Deduced by Electrochemical and Structural Analyses, J Electrochem Soc, 157 (2010) A499-A507.

[69] E. Markervich, G. Salitra, M.D. Levi, D. Aurbach, Capacity Fading of Lithiated Graphite Electrodes Studied by a Combination of Electroanalytical Methods, Raman Spectroscopy and SEM, J Power Sources, 146 (2005) 146-150.

[70] R. Deshpande, M. Verbrugge, Y.T. Cheng, J. Wang, P. Liu, Battery Cycle Life Prediction with Coupled Chemical Degradation and Fatigue Mechanics, J Electrochem Soc, 159 (2012) A1730-A1738.

[71] M. Broussely, P. Biensan, F. Bonhomme, P. Blanchard, S. Herreyre, K. Nechev, R.J. Staniewicz, Main Aging Mechanisms in Li Ion Batteries, J Power Sources, 146 (2005) 90-96.

[72] R. Spotnitz, Simulation of Capacity Fade in Lithium-Ion Batteries, J Power Sources, 113 (2003) 72-80.

[73] J. Christensen, J. Newman, Stress Generation and Fracture in Lithium Insertion Materials, J Solid State Electr, 10 (2006) 293-319.

[74] X.C. Zhang, W. Shyy, A.M. Sastry, Numerical Simulation of Intercalation-Induced Stress in Li-Ion Battery Electrode Particles, J Electrochem Soc, 154 (2007) A910-A916.

[75] X.C. Zhang, A.M. Sastry, W. Shyy, Intercalation-Induced Stress and Heat Generation within Single Lithium-Ion Battery Cathode Particles, J Electrochem Soc, 155 (2008) A542-A552.

[76] J. Christensen, J. Newman, A Mathematical Model of Stress Generation and Fracture in Lithium Manganese Oxide, J Electrochem Soc, 153 (2006) A1019-A1030.

[77] R. Deshpande, Y. Qi, Y.T. Cheng, Effects of Concentration-Dependent Elastic Modulus on Diffusion-Induced Stresses for Battery Applications, J Electrochem Soc, 157 (2010) A967-A971.

[78] R. Deshpande, Y.T. Cheng, M.W. Verbrugge, Modeling Diffusion-Induced Stress in Nanowire Electrode Structures, J Power Sources, 195 (2010) 5081-5088.

[79] R. Deshpande, Y.T. Cheng, M.W. Verbrugge, A. Timmons, Diffusion Induced Stresses and Strain Energy in a Phase-Transforming Spherical Electrode Particle, J Electrochem Soc, 158 (2011) A718-A724.

[80] V.A. Sethuraman, N. Van Winkle, D.P. Abraham, A.F. Bower, P.R. Guduru, Real-Time Stress Measurements in Lithium-Ion Battery Negative-Electrodes, J Power Sources, 206 (2012) 334-342.

[81] W.Q. Lu, A. Jansen, D. Dees, P. Nelson, N.R. Veselka, G. Henriksen, High-Energy Electrode Investigation for Plug-In Hybrid Electric Vehicles, J Power Sources, 196 (2011) 1537-1540.

[82] G. Liu, H. Zheng, S. Kim, Y. Deng, A.M. Minor, X. Song, V.S. Battaglia, Effects of Various Conductive Additive and Polymeric Binder Contents on the Performance of a Lithium-Ion Composite Cathode, J Electrochem Soc, 155 (2008) A887-A892.

[83] P. Nelson, I. Bloom, K. Amine, G. Henriksen, Design Modeling of Lithium-Ion Battery Performance, J Power Sources, 110 (2002) 437-444.

[84] J. Shim, K.A. Striebel, Effect of Electrode Density on Cycle Performance and Irreversible Capacity Loss for Natural Graphite Anode in Lithium-Ion Batteries, J Power Sources, 119 (2003) 934-937.

[85] H.H. Zheng, J. Li, X.Y. Song, G. Liu, V.S. Battaglia, A Comprehensive Understanding of Electrode Thickness Effects on the Electrochemical Performances of Li-Ion Battery Cathodes, Electrochim Acta, 71 (2012) 258-265.

[86] V. Srinivasan, J. Newman, Design and Optimization of a Natural Graphite/Iron Phosphate Lithium-Ion Cell, J Electrochem Soc, 151 (2004) A1530-A1538.

[87] Y.H. Chen, C.W. Wang, X. Zhang, A.M. Sastry, Porous Cathode Optimization for Lithium Cells: Ionic and Electronic Conductivity, Capacity, and Selection of Materials, J Power Sources, 195 (2010) 2851-2862.

[88] H.H. Zheng, R.Z. Yang, G. Liu, X.Y. Song, V.S. Battaglia, Cooperation between Active Material, Polymeric Binder and Conductive Carbon Additive in Lithium Ion Battery Cathode, J Phys Chem C, 116 (2012) 4875-4882.

[89] G. Liu, H. Zheng, A.S. Simens, A.M. Minor, X. Song, V.S. Battaglia, Optimization of Acetylene Black Conductive Additive and PVDF Composition for High-Power Rechargeable Lithium-Ion Cells, J Electrochem Soc, 154 (2007) A1129-A1134.

[90] J.M. Tarascon, D. Guyomard, The $Li_{1+x}Mn_2O_4$/C Rocking-Chair System - A Review, Electrochim Acta, 38 (1993) 1221-1231.

[91] D. Guyomard, J.M. Tarascon, The Carbon/$Li_{1+x}Mn_2O_4$ System, Solid State Ionics, 69 (1994) 222-237.

[92] R.J. Xue, H. Huang, G.B. Li, L.Q. Chen, Effect of Cathode Anode Mass-Ratio in Lithium-Ion Secondary Cells, J Power Sources, 55 (1995) 111-114.

[93] P. Arora, R.E. White, M. Doyle, Capacity Fade Mechanisms and Side Reactions in Lithium-Ion Batteries, J Electrochem Soc, 145 (1998) 3647-3667.

[94] B. Son, M.H. Ryou, J. Choi, S.H. Kim, J.M. Ko, Y.M. Lee, Effect of Cathode/Anode Area Ratio on Electrochemical Performance of Lithium-Ion Batteries, J Power Sources, 243 (2013) 641-647.

[95] R.A. Huggins, Advanced Batteries : Materials Science Aspects, Springer, New York, 2008.

[96] J.G. Xu, R.D. Deshpande, J. Pan, Y.T. Cheng, V.S. Battaglia, Electrode Side Reactions, Capacity Loss and Mechanical Degradation in Lithium-Ion Batteries, J Electrochem Soc, 162 (2015) A2026-A2035.

[97] A.J. Smith, J.C. Burns, D. Xiong, J.R. Dahn, Interpreting High Precision Coulometry Results on Li-ion Cells, J Electrochem Soc, 158 (2011) A1136-A1142.

[98] R.D. Deshpande, P. Ridgway, Y.B. Fu, W. Zhang, J.S. Cai, V. Battaglia, The Limited Effect of VC in Graphite/NMC Cells, J Electrochem Soc, 162 (2015) A330-A338.

[99] P.T. Kissinger, W.R. Heineman, Cyclic Voltammetry, J Chem Educ, 60 (1983) 702-706.

[100] P. Van der Heide, X-ray Photoelectron Spectroscopy : An Introduction to Principles and Practices, Wiley, Hoboken, N.J., 2012.

[101] M.N. Obrovac, L. Christensen, Structural Changes in Silicon Anodes during Lithium Insertion/Extraction, Electrochem Solid St, 7 (2004) A93-A96.

[102] Z.J. Cai, Y.B. Liu, S.S. Liu, L. Li, Y.M. Zhang, High Performance of Lithium-Ion Polymer Battery Based on Non-Aqueous Lithiated Perfluorinated Sulfonic Ion-Exchange Membranes, Energ Environ Sci, 5 (2012) 5690-5693.

[103] D. Mazouzi, Z. Karkar, C.R. Hernandez, P.J. Manero, D. Guyomard, L. Roue, B. Lestriez, Critical Roles of Binders and Formulation at Multiscales of Silicon-Based Composite Electrodes, J Power Sources, 280 (2015) 533-549.

[104] A. Magasinski, B. Zdyrko, I. Kovalenko, B. Hertzberg, R. Burtovyy, C.F. Huebner, T.F. Fuller, I. Luzinov, G. Yushin, Toward Efficient Binders for Li-Ion Battery Si-Based Anodes: Polyacrylic Acid, Acs Appl Mater Inter, 2 (2010) 3004-3010.

[105] W.R. Liu, M.H. Yang, H.C. Wu, S.M. Chiao, N.L. Wu, Enhanced Cycle Life of Si Anode for Li-Ion Batteries by Using Modified Elastomeric Binder, Electrochem Solid St, 8 (2005) A100-A103.

[106] H. Buqa, M. Holzapfel, F. Krumeich, C. Veit, P. Novák, Study of Styrene Butadiene Rubber and Sodium Methyl Cellulose as Binder for Negative Electrodes in Lithium-Ion Batteries, J Power Sources, 161 (2006) 617-622.

[107] B. Lestrie, S. Bahri, I. Sandu, L. Roue, D. Guyomard, On the Binding Mechanism of CMC in Si Negative Electrodes for Li-Ion Batteries, Electrochem Commun, 9 (2007) 2801-2806.

[108] N.S. Hochgatterer, M.R. Schweiger, S. Koller, P.R. Raimann, T. Wohrle, C. Wurm, M. Winter, Silicon/Graphite Composite Electrodes for High-Capacity Anodes: Influence of Binder Chemistry on Cycling Stability, Electrochem Solid St, 11 (2008) A76-A80.

[109] D. Mazouzi, B. Lestriez, L. Roue, D. Guyomard, Silicon Composite Electrode with High Capacity and Long Cycle Life, Electrochem Solid St, 12 (2009) A215-A218.

[110] I. Kovalenko, B. Zdyrko, A. Magasinski, B. Hertzberg, Z. Milicev, R. Burtovyy, I. Luzinov, G. Yushin, A Major Constituent of Brown Algae for Use in High-Capacity Li-Ion Batteries, Science, 334 (2011) 75-79.

[111] M. Murase, N. Yabuuchi, Z.J. Han, J.Y. Son, Y.T. Cui, H. Oji, S. Komaba, Crop-Derived Polysaccharides as Binders for High-Capacity Silicon/Graphite-Based Electrodes in Lithium-Ion Batteries, Chemsuschem, 5 (2012) 2307-2311.

[112] Q.W. Tang, Z.Q. Shan, L. Wang, X. Qin, K.L. Zhu, J.H. Tian, X.S. Liu, Nafion Coated Sulfur-Carbon Electrode for High Performance Lithium-Sulfur Batteries, J Power Sources, 246 (2014) 253-259.

[113] Y.B. Liu, Z.J. Cai, L. Tan, L. Li, Ion Exchange Membranes as Electrolyte for High Performance Li-Ion Batteries, Energ Environ Sci, 5 (2012) 9007-9013.

[114] Z.Q. Jin, K. Xie, X.B. Hong, Z.Q. Hu, X. Liu, Application of Lithiated Nafion Ionomer Film as Functional Separator for Lithium Sulfur Cells, J Power Sources, 218 (2012) 163-167.

[115] H.Y. Liang, X.P. Qiu, S.C. Zhang, W.T. Zhu, L.Q. Chen, Study of Lithiated Nafion Ionomer for Lithium Batteries, J Appl Electrochem, 34 (2004) 1211-1214.

[116] A.M. Chockla, T.D. Bogart, C.M. Hessel, K.C. Klavetter, C.B. Mullins, B.A. Korgel, Influences of Gold, Binder and Electrolyte on Silicon Nanowire Performance in Li-Ion Batteries, J Phys Chem C, 116 (2012) 18079-18086.

[117] M.N. Obrovac, L.J. Krause, Reversible Cycling of Crystalline Silicon Powder, J Electrochem Soc, 154 (2007) A103-A108.

[118] K.W. Schroder, H. Celio, L.J. Webb, K.J. Stevenson, Examining Solid Electrolyte Interphase Formation on Crystalline Silicon Electrodes: Influence of Electrochemical Preparation and Ambient Exposure Conditions, J Phys Chem C, 116 (2012) 19737-19747.

[119] H. Nakai, T. Kubota, A. Kita, A. Kawashima, Investigation of the Solid Electrolyte Interphase Formed by Fluoroethylene Carbonate on Si Electrodes, J Electrochem Soc, 158 (2011) A798-A801.

[120] N.S. Choi, K.H. Yew, K.Y. Lee, M. Sung, H. Kim, S.S. Kim, Effect of Fluoroethylene Carbonate Additive on Interfacial Properties of Silicon Thin-Film Electrode, J Power Sources, 161 (2006) 1254-1259.

[121] K. Feng, B.B. Tang, P.Y. Wu, Ammonia-Assisted Dehydrofluorination between PVDF and Nafion for Highly Selective and Low-Cost Proton Exchange Membranes: A Possible Way to further Strengthen the Commercialization of Nafion, J Mater Chem A, 3 (2015) 12609-12615.

[122] B. Philippe, R. Dedryvere, J. Allouche, F. Lindgren, M. Gorgoi, H. Rensmo, D. Gonbeau, K. Edstrom, Nanosilicon Electrodes for Lithium-Ion Batteries: Interfacial Mechanisms Studied by Hard and Soft X-ray Photoelectron Spectroscopy, Chem Mater, 24 (2012) 1107-1115.

[123] D. Aurbach, Review of Selected Electrode-Solution Interactions which Determine the Performance of Li and Li Ion Batteries, J Power Sources, 89 (2000) 206-218.

[124] V. Etacheri, O. Haik, Y. Goffer, G.A. Roberts, I.C. Stefan, R. Fasching, D. Aurbach, Effect of Fluoroethylene Carbonate (FEC) on the Performance and Surface Chemistry of Si-Nanowire Li-Ion Battery Anodes, Langmuir, 28 (2012) 965-976.

[125] Q.L. Zhang, X.C. Xiao, W.D. Zhou, Y.T. Cheng, M.W. Verbrugge, Toward High Cycle Efficiency of Silicon-Based Negative Electrodes by Designing the Solid Electrolyte Interphase, Adv Energy Mater, 5 (2015).

[126] N. Dupré, P. Moreau, E. De Vito, L. Quazuguel, M. Boniface, A. Bordes, C. Rudisch, P. Bayle-Guillemaud, D. Guyomard, Multiprobe Study of the Solid Electrolyte Interphase on Silicon-Based Electrodes in Full-Cell Configuration, Chem Mater, 28 (2016) 2557-2572.

[127] Y. Oumellal, N. Delpuech, D. Mazouzi, N. Dupré, J. Gaubicher, P. Moreau, P. Soudan, B. Lestriez, D. Guyomard, The Failure Mechanism of Nano-Sized Si-Based Negative Electrodes for Lithium Ion Batteries, J Mater Chem, 21 (2011) 6201-6208.

[128] J.R. Szczech, S. Jin, Nanostructured Silicon for High Capacity Lithium Battery Anodes, Energ Environ Sci, 4 (2011) 56-72.

[129] L.Y. Shen, Z.X. Wang, L.Q. Chen, Carbon-Coated Hierarchically Porous Silicon as Anode Material for Lithium Ion Batteries, Rsc Adv, 4 (2014) 15314-15318.

[130] T. Chen, Q. Zhang, J. Xu, J. Pan, Y.T. Cheng, Binder-Free Lithium Ion Battery Electrodes Made of Silicon and Pyrolized Lignin, Rsc Adv, 6 (2016) 29308-29313.

[131] S. Dalavi, P. Guduru, B.L. Lucht, Performance Enhancing Electrolyte Additives for Lithium Ion Batteries with Silicon Anodes, J Electrochem Soc, 159 (2012) A642-A646.

[132] M.T. Jeena, J.I. Lee, S.H. Kim, C. Kim, J.Y. Kim, S. Park, J.H. Ryu, Multifunctional Molecular Design as an Efficient Polymeric Binder for Silicon Anodes in Lithium-Ion Batteries, Acs Appl Mater Inter, 6 (2014) 18001-18007.

[133] H. Zhao, Y. Wei, R. Qiao, C. Zhu, Z. Zheng, M. Ling, Z. Jia, Y. Bai, Y. Fu, J. Lei, Conductive Polymer Binder for High-Tap-Density Nanosilicon Material for Lithium-Ion Battery Negative Electrode Application, Nano Lett, 15 (2015) 7927-7932.

[134] T.M. Higgins, S.-H. Park, P.J. King, C. Zhang, N. McEvoy, N.C. Berner, D. Daly, A. Shmeliov, U. Khan, G. Duesberg, A Commercial Conducting Polymer as Both Binder and Conductive Additive for Silicon Nanoparticle-Based Lithium-Ion Battery Negative Electrodes, Acs Nano, 10 (2016) 3702-3713.

[135] J. Xu, Q. Zhang, Y.T. Cheng, High Capacity Silicon Electrodes with Nafion as Binders for Lithium-Ion Batteries, J Electrochem Soc, 163 (2016) A401-A405.

[136] M.N. Obrovac, L. Christensen, D.B. Le, J.R. Dahnb, Alloy Design for Lithium-Ion Battery Anodes, J Electrochem Soc, 154 (2007) A849-A855.

[137] N. Delpuech, N. Dupre, P. Moreau, J.S. Bridel, J. Gaubicher, B. Lestriez, D. Guyomard, Mechanism of Silicon Electrode Aging upon Cycling in Full Lithium-Ion Batteries, Chemsuschem, 9 (2016) 841-848.

[138] E. Radvanyi, W. Porcher, E. De Vito, A. Montani, S. Franger, S.J.S. Larbi, Failure Mechanisms of Nano-Silicon Anodes upon Cycling: An Electrode Porosity Evolution Model, Phys Chem Chem Phys, 16 (2014) 17142-17153.

[139] X.H. Liu, L. Zhong, S. Huang, S.X. Mao, T. Zhu, J.Y. Huang, Size-Dependent Fracture of Silicon Nanoparticles during Lithiation, Acs Nano, 6 (2012) 1522-1531.

[140] Z.S. Ma, T.T. Li, Y.L. Huang, J. Liu, Y.C. Zhou, D.F. Xue, Critical Silicon-Anode Size for Averting Lithiation-Induced Mechanical Failure of Lithium-Ion Batteries, Rsc Adv, 3 (2013) 7398-7402.

[141] C. Wang, H. Wu, Z. Chen, M.T. McDowell, Y. Cui, Z.A. Bao, Self-Healing Chemistry Enables the Stable Operation of Silicon Microparticle Anodes for High-Energy Lithium-Ion Batteries, Nat Chem, 5 (2013) 1043-1049.

Vita

Education

University of Science and Technology Beijing, M.E. Materials Science, 2011

University of Science and Technology Beijing, B.E. Materials Science and Engineering, 2008

Publications

[1] T. Chen, Q. Zhang, J. Pan, J. Xu, Y. Liu, M. Ah-Shroofy, Y.T. Cheng, Low-Temperature Treated Lignin as Both Binder and Conductive Additive for Silicon Nanoparticle Composite Electrodes in Lithium-Ion Batteries, *Accepted by ACS Applied Materials & Interfaces, in press.*

[2] T. Chen, Q. Zhang, J. Xu, J. Pan, Y.T. Cheng, Binder-Free Lithium Ion Battery Electrodes Made of Silicon and Pyrolized Lignin, *Rsc Adv*, **6** (2016) 29308-29313.

[3] J. Xu, Q. Zhang, Y.T. Cheng, High Capacity Silicon Electrodes with Nafion as Binders for Lithium-Ion Batteries, *J Electrochem Soc*, **163** (2016) A401-A405.

[4] J. Xu, R.D. Deshpande, J. Pan, Y.T. Cheng, V.S. Battaglia, Electrode Side Reactions, Capacity Loss and Mechanical Degradation in Lithium-Ion Batteries, *J Electrochem Soc*, **162** (2015) A2026-A2035.